Accepted Manuscript

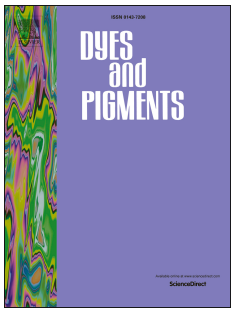

Donor–acceptor–acceptor-based non-fullerene acceptors comprising terminal chromen-2-one functionality for efficient bulk-heterojunction devices

Pedada Srinivasa Rao, Akhil Gupta, Sidhanath V. Bhosale, Ante Bilic, Wanchun Xiang, Richard A. Evans, Sheshanath V. Bhosale

PII: S0143-7208(17)31088-4

DOI: 10.1016/j.dyepig.2017.07.047

Reference: DYPI 6136

To appear in: *Dyes and Pigments*

Received Date: 10 May 2017

Revised Date: 20 July 2017

Accepted Date: 20 July 2017

Please cite this article as: Srinivasa Rao P, Gupta A, Bhosale SV, Bilic A, Xiang W, Evans RA, Bhosale SV, Donor–acceptor–acceptor-based non-fullerene acceptors comprising terminal chromen-2-one functionality for efficient bulk-heterojunction devices, *Dyes and Pigments* (2017), doi: 10.1016/j.dyepig.2017.07.047.

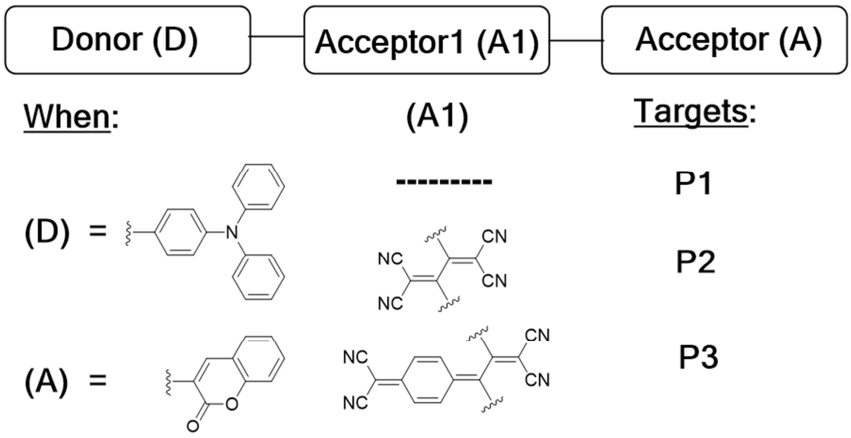

Non-fullerene electron acceptors P1, P2 and P3

Donor–acceptor–acceptor-based non-fullerene acceptors comprising terminal chromen-2-one functionality for efficient bulk-heterojunction devices

Pedada Srinivasa Rao,[a,b] Akhil Gupta,*[c] Sidhanath V. Bhosale,*[a] Ante Bilic,[d] Wanchun Xiang,[e] Richard A. Evans[f] and Sheshanath V. Bhosale*[g]

a Polymers and Functional Materials Division, CSIR-Indian Institute of Chemical Technology, Hyderabad 500007, Telangana, India; Email: bhosale@iict.res.in

b Academy of Scientific and Innovative Research (AcSIR), CSIR-IICT, Hyderabad 500007, Telangana, India

c Institute for Frontier Materials, Deakin University, Waurn Ponds, Victoria 3216 Australia; Tel: +61 3 5247 9542; E-mail: akhil.gupta@deakin.edu.au

d Data61 CSIRO, Molecular and Materials Modelling, Docklands, Victoria 8012 Australia

e State Key Laboratory of Silicate Materials for Architectures, Wuhan University of Technology, 122 Luoshi Rd, Wuhan 430070 Hubei, P. R. China

f CSIRO Manufacturing, Bayview Avenue, Clayton South, Victoria 3169 Australia

g School of Science, RMIT University, GPO Box 2476, Melbourne Victoria 3001 Australia; Tel: +61 3 9925 2680; E-mail: sheshanath.bhosale@rmit.edu.au

Abstract

Two simple semiconducting donor–acceptor–acceptor (D–A_1–A) modular, small molecule, non-fullerene electron acceptors, 2-(4-(diphenylamino)phenyl)-3-(4-((2-oxo-2*H*-chromen-3-yl)ethynyl)phenyl)buta-1,3-diene-1,1,4,4-tetracarbonitrile (**P2**) and 2-(4-(3,3-dicyano-1-(4-(diphenylamino)phenyl)-2-(4-((2-oxo-2*H*-chromen-3-yl)ethynyl)phenyl)allylidene)cyclohexa-2,5-dien-1-ylidene)malononitrile (**P3**), were designed, synthesized and characterized for application in solution-processable bulk-heterojunction solar cells. The optoelectronic and photovoltaic properties of **P2** and **P3** were directly compared with those of a structural analogue, 3-((4-((4-(diphenylamino)phenyl)ethynyl)phenyl)ethynyl)-2*H*-chromen-2-one (**P1**), which was designed based on a D–A format. All of these new materials comprised an electron rich triphenylamine (TPA) donor core (D) and electron deficient chromen-2-one terminal core (A). In the simple D–A system, TPA and chromenone were the terminal functionalities, whereas in the D–A_1–A system, tetracyanoethylene (TCNE) and tetracyanoquinodimethane (TCNQ) derived functionalities were incorporated as A_1 units by keeping the D/A units constant. The inclusion of A_1 was primarily done to induce cross-conjugation within the molecular backbone and hence to generate low band gap targets. The physical and optoelectronic properties were characterised by ultraviolet–visible (UV–Vis), thermogravimetric analysis, photo-electron spectroscopy in air and cyclic voltammetry. These new materials exhibited broadened absorption spectra, for instance panchromatic absorbance in case of **P3**, excellent solubility and thermal stability, and energy levels matching those of the conventional and routinely used donor polymer poly(3-hexyl thiophene) (P3HT). Solution-processable bulk-heterojunction devices were fabricated with **P1**, **P2** and **P3** as non-fullerene electron acceptors. Studies on the photovoltaic properties revealed that the best P3HT: **P3**-based device showed an impressive enhanced power

conversion efficiency of 4.21%, an increase of around two-fold with respect to the efficiency of the best P3HT: **P1**-based device (2.28%). Our results clearly demonstrate that the D–A_1–A type small molecules are promising non-fullerene electron acceptors in the research field of organic solar cells.

Keywords: solution-processable; triphenylamine; chromen-2-one; bulk-heterojunction; donor–acceptor–acceptor; solar cells

1. Introduction

There is a constant demand for the development of renewable technologies as humanity is progressing through 21st century. The survival of the human race is often associated with the supply of endless energy resources, and the natural resources such as wind, sunlight and water can provide a definitive answer. Of such natural resources, sunlight or solar power seems to be a strong candidate given the fact that our sun is still in its young age. Utilization of solar energy or photovoltaic effect can in fact be dated back to Becquerel's 1839 work when he observed similar effects while studying liquid electrolytes [1]. However, developmental work to fabricate solar cell devices started with Tang's 1989 work [2] and provided a proof of concept that a variety of organic, inorganic or even tandem solar cells can be a reality in the near future. Since then, a variety of solar cells have been designed, fabricated, and have shown that the solar power indeed is the way to go as far as renewable technologies are concerned. Among such solar cells, organic, or otherwise termed bulk-heterojunction, solar cells [3] and dye sensitized solar cells [4] are the most studied, well understood and widely accepted strategies. As far as bulk-heterojunction (BHJ) devices are concerned, two types of developments – materials and device fabrication – have attracted considerable attention over the past two decades. Therefore, it is apparent that this technology

is worth studying and developing given the fact that such devices do promise multiple advantages such as light weight, low cost and flexibility [5–7].

A typical BHJ architecture is an interlaced network of organic donor and acceptor semiconducting materials which is formed during device fabrication mainly via solution processing. Conventionally, semiconducting donor polymers, such as poly(3-hexylthiophene) (P3HT), and acceptors, such as fullerene derivatives, either [6,6]-phenyl-C_{61}-butyric acid methyl ester ($PC_{61}BM$) or its C_{71} analogue ($PC_{71}BM$), have been employed to attain a strong understanding of material design and device morphology [5–7]. As a result, conjugated polymers and small molecules as alternative donors, and non-fullerene acceptors as alternative accepting functionalities have been developed over time. It is judicious to point out that the fullerene derivatives have been extensively used as acceptor materials due to their intrinsic properties such as high electron affinity, isotropy of charge transport, and the ability to form favourable nanoscale networks with a variety of donor materials [8–10]. Despite the fact that fullerene acceptors are dominant in the research field of organic photovoltaics and have been widely explored, they are visibly afflicted with a number of potential limitations such as weak absorption in the visible spectrum, poor photo-stability in air, and restricted electronic tuning via structural modification, to name a few [11,12]. Moreover, a large electron affinity can result in low open-circuit voltage [13]. Such disadvantages with fullerenes provide a strong support to the fact that alternate structural formats must be designed and developed, for instance non-fullerene acceptors, which not only exhibit most of the properties that make fullerene acceptors appealing but must satisfy the requirements such as efficient absorption over visible spectrum, excellent solubility, high charge carrier mobility and matching energy levels with those of a variety of donors.

It is evident that past few years have seen a dramatic surge in the development of non-fullerene acceptors. High power conversion efficiency (PCE) numbers, typically ranging 11–12%, have been reported so far for organic solar cells based on non-fullerene acceptors [14,15]. Though this advancement is encouraging, incentives remain to develop materials which will not only have better properties than fullerenes, but will also have crucial characteristics such as solubility, chemical and thermal stability, and matching energy levels with donors. Moreover, a newly designed non-fullerene acceptor should be compatible with the commercially available polymeric donors such as P3HT. As per our understanding of this research area, we theorize that a potential non-fullerene acceptor must be a conjugated structure, either via the conjunction of a variety of building blocks (primarily donors and acceptors) or should possess a rigid, extended fused-ring backbone. The advantages of using donor/acceptor, or otherwise termed push/pull, functionalities lie in the fact that the combination of such formats can reduce the optical bandgap, broaden absorption in the entire visible region of the solar spectrum, and tune energy levels.

Having said this, we and others have been successful in demonstrating the use of a number of push/pull formats to design a number of potential non-fullerene electron acceptors where such targets have displayed promising device performance [16–34]. We realised that functionalities such as triphenylamine (TPA), diketopyrrolopyrrole (DPP), naphthalenediimide (NDI), and more recently, functionalities which contain cyano groups, such as dicyanoindenedione, tetracyanoethylene (TCNE) and tetracyanoquinodimethane (TCNQ), are promising building blocks (donors and acceptors), and have been used in recent past. However, their amalgamation can be done in a variety of fashions. In this contribution, we wish to report a new combination where we have used a new acceptor unit, 2-chromenone, along with the terminal donor TPA. Overall, three targets were designed based

on TPA- and chromenone-functionalized molecular systems of the types D–A and D–A_1–A. In the simple D–A system, TPA and chromenone were the terminal functionalities, whereas in the D–A_1–A system, TCNE and TCNQ derived functionalities were incorporated as A_1 units by keeping the D/A units constant. It has been shown in the literature that cross-conjugation is an efficient strategy to design low highest occupied molecular orbital–lowest unoccupied molecular orbital (HOMO–LUMO) gap molecular systems [35–37]. Moreover, the presence of cyano group in a molecular backbone can promote the formation of a crystallite architecture and can increase electron affinity, thereby favouring efficient charge transport and broadening absorption profile towards a longer wavelength region, near infrared in particular. Such advantages are likely responsible for generating a focused interest in designing of chromophores based on accepting units comprising cyano groups, and are an inspiration to pursue research on the development of new and potential non-fullerene electron acceptors.

Fig. 1 reveals the molecular structures of new materials, 3-((4-((4-(diphenylamino)phenyl)ethynyl)phenyl)ethynyl)-2*H*-chromen-2-one (**P1**), 2-(4-(diphenylamino)phenyl)-3-(4-((2-oxo-2*H*-chromen-3-yl)ethynyl)phenyl)buta-1,3-diene-1,1,4,4-tetracarbonitrile (**P2**) and 2-(4-(3,3-dicyano-1-(4-(diphenylamino)phenyl)-2-(4-((2-oxo-2*H*-chromen-3-yl)ethynyl)phenyl)allylidene)cyclohexa-2,5-dien-1-ylidene)malononitrile (**P3**), where **P1** was based on the D–A type, and **P2** and **P3** were based on the D–A_1–A modular design. The optoelectronic and photovoltaic properties of **P2** and **P3** were directly compared with **P1**. It was observed that the introduction of TCNE and TCNQ functionalities in **P2** and **P3**, respectively, resulted in strong intramolecular charge transfer transition when compared with **P1**. The introduction of TCNQ in particular exhibited a broader absorption profile extending up to 1000 nm, primarily ascribed to the stronger electron withdrawing

nature of TCNQ relative to TCNE. Both **P2** and **P3** exerted low optical band gaps and low lying HOMO energy levels when compared with **P1**. All of the investigated materials displayed high chemical and thermal stability, and excellent solubility. Solution-processable BHJ devices were fabricated with **P1**, **P2** and **P3** as non-fullerene electron acceptors. Studies on the photovoltaic properties revealed that the best P3HT: **P3**-based device showed an impressive enhanced power conversion efficiency of 4.21%, an increase of greater than two-fold with respect to the efficiency of the best P3HT: **P1**-based device (2.28%). To our knowledge, there are no reports on the connected use of TPA and 2-chromenone functionalities where such functionalities have been used to design non-fullerene acceptor formats comprising either TCNE or TCNQ units. Our results indicate that these 2-chromenone-based small molecules are potential acceptors for efficient organic solar cells using a commercially available donor polymer P3HT and can further be explored with a variety of donors. The present work is a continuation of our efforts made in the design and development of small molecular chromophores for organic photovoltaic applications [38–41].

>Fig. 1<

2. Experimental details

2.1. Materials, methods and device details

All the reagents and chemicals used, unless otherwise specified, were purchased from Sigma-Aldrich Co., Bengaluru, Karnataka, India, and were used without any purification. AR grade solvents were purchased from Finar chemicals Limited, India and used as received. ^{1}H and ^{13}C NMR spectra were recorded at 300, 400 or 500 MHz as indicated. The following abbreviations were used to explain multiplicities: s = singlet, d = doublet, t = triplet, q = quartet, m = multiplet, br = broad, dd = doublet of doublets, and dt = doublet of triplets. ^{13}C

NMR spectra were recorded at 75 or 101 MHz, as indicated. ^{1}H and ^{13}C chemical shifts were calibrated using residual non-deuterated solvent as an internal reference and are reported in parts per million (δ) relative to tetramethylsilane (δ = 0). All experiments were performed in deuterated chloroform ($CDCl_3$). ESI was used to ionize samples with a spray voltage. The mass spectrometry measurements were performed using either Fourier transform-based high resolution mass spectrometry or via atmospheric-pressure chemical ionization (APCI) experiments which were carried out on FTMS, ionized by APCI from an atmospheric solids analysis probe (ASAP). FTIR spectra were recorded using Thermo Nicolet Nexus 670 spectrometer in the form of non-hygroscopic KBr pellets. The UV–Vis spectra were recorded using a Shimadzu UV-1800 spectrophotometer at room temperature. The TGA experiments were carried out using Q-500 TGA instrument with nitrogen as a purging gas. The samples were heated to 800 °C at 10 °C/minute under nitrogen atmosphere. AFM topographic maps were performed directly on the active layers of P3HT: **P1**/**P2**/**P3** blends using an Asylum Research MFP-3D-SA instrument. The AFM was run in intermittent contact mode (tapping mode) using MicroMasch NSC18 tips (typical resonant frequency ~100 kHz, typical probe radius ~10 nm and typical aspect ratio 3:1). Transmission electron microscopy samples were prepared by solvent evaporation on a holey carbon grid and micrographs were produced using a JOEL 1010 100 kV TEM.

Though the general details of spectroscopic measurements and characterization were reported previously [42], specific details of device fabrication are reported herein. Indium tin oxide (ITO)-coated glass (Kintek, 15 Ohms per square) was cleaned by standing in a stirred solution of 5% (*v*/*v*) Deconex 12PA detergent at 90 °C for 20 minutes. The ITO-coated glass was then successively sonicated for 10 min each in distilled water, acetone and isopropanol. The substrates were then exposed to a UV–ozone clean at room temperature for 10 min. UV/ozone cleaning of glass substrates was performed using a Novascan PDS-UVT,

UV/ozone cleaner with the platform set to maximum height. The intensity of the lamp was greater than 36 mW/cm^2 at a distance of 10 cm. At ambient conditions the ozone output of the UV cleaner is greater than 50 ppm. Aqueous solutions of PEDOT/PSS (HC Starck, Baytron P AI 4083) were filtered (0.2 µm RC filter) and deposited onto glass substrates in air by spin coating (Laurell WS-400B-6NPP lite single wafer spin processor) at 5000 rpm for 60 s to give a layer having a thickness of 40 ± 5 nm. The PEDOT/PSS layer was then annealed on a hotplate in a glove box at 145 °C for 10 min. For OPV devices, the newly synthesized organic *n*-type materials and P3HT were dissolved in individual vials by magnetic stirring. Blend ratios and solution concentrations were varied to optimize device performance. The solutions were then combined, filtered (0.2 µm RC filter) and deposited by spin coating onto the ITO-coated glass substrates inside a glove box. The coated substrates were then transferred (without exposure to air) to a vacuum evaporator inside an adjacent nitrogen-filled glove box. Samples were placed on a shadow mask in a tray. The area defined by the shadow mask gave device areas of exactly 0.2 cm^2. Deposition rates and film thicknesses were monitored using a calibrated quartz thickness monitor inside the vacuum chamber. Layers of calcium (Ca) (Aldrich) and aluminium (Al) (3 pellets of 99.999%, KJ Lesker) having thicknesses of 20 nm and 100 nm, respectively, were evaporated from open tungsten boats onto the active layer by thermal evaporation at pressures less than 2×10^{-6} mbar. A connection point for the ITO electrode was made by manually scratching off a small area of the active layers. A small amount of silver paint (Silver Print II, GC Electronics, part no.: 22-023) was then deposited onto all of the connection points, both ITO and Al. The completed devices were then encapsulated with glass and a UV-cured epoxy (Summers Optical, Lens Bond type J-91) by exposing to 365 nm UV light inside a glove box for 10 min. The encapsulated devices were then removed from the glove box and tested in air within 1 h. The OPV devices were tested using an Oriel solar simulator fitted with a 1000 W xenon lamp

filtered to give an output of 100 mW/cm^2 at simulated AM 1.5. The lamp was calibrated using a standard, filtered silicon (Si) cell from Peccell Limited which was subsequently cross-calibrated with a standard reference cell traceable to the National Renewable Energy Laboratory. The devices were tested using a Keithley 2400 Sourcemeter controlled by labview software. Film thicknesses were determined using a Dektak 6M Profilometer.

2.2. Synthesis and characterization

Compound **P1** was synthesized by reacting 4-((4-ethynylphenyl)ethynyl)-*N*,*N*-diphenylaniline (compound **6**) with 3-iodo-2*H*-chromen-2-one using Sonogashira coupling reaction in dry tetrahydrofuran (THF) (Scheme 1). Compounds **P2** and **P3** were synthesized by reacting **P1** with TCNE and TCNQ, respectively (Scheme 2). The final compounds were purified using silica gel chromatography, characterized spectrally, and their physical properties were investigated. The materials were prepared in moderate to high yields and were found to be highly soluble in a variety of conventional organic solvents such as chlorobenzene, chloroform, dichloromethane and toluene. High solubility of organic materials is an essential criterion for the fabrication of solution-processable organic photovoltaic devices and newly designed materials **P1**, **P2** and **P3** fulfil this criterion. The compounds **2**, **3** and **4** were synthesised following the procedures reported in the literature [43–44].

>Scheme 1<

>Scheme 2<

*2.2.1 Synthesis of N,N-diphenyl-4-((4-((triisopropylsilyl)ethynyl)phenyl)ethynyl)aniline (**5**)*

To the stirred solution of compound **4** (2.00 g, 7.07 mmol) in dry toluene (30 mL) was added 4-iodotriphenylamine (2.62 g, 7.07 mmol), and the resulting reaction solution was stirred for 15 min under nitrogen atmosphere. *N*,*N*–diisopropylethylamine and catalytic amounts of

bis(triphenylphosphine)palladium(II) chloride and copper iodide (ca. 5 mol% each) were added to the reaction mixture. The reaction mixture was stirred overnight at room temperature. After the completion of reaction (TLC monitoring), solvent was removed under reduced pressure and the crude product was purified via silica gel column chromatography (eluent: hexane) to afford compound **5** as a colourless liquid (3.30 g, yield: 91%). FTIR (neat; cm^{-1}): 3441, 2942, 2864, 2210, 2152, 1706, 1513, 1493, 1315, 1281, 1017, 835, 753, 696, 673, 507; ^{1}H NMR (400 MHz, $CDCl_3$) δ 7.42 (s, 4H), 7.37 (d, J = 8.8 Hz, 2H), 7.29–7.27 (m, 4H), 7.12 (d, J = 7.4 Hz, 4H), 7.08 (t, J = 7.3 Hz, 2H), 7.00 (d, J = 8.8 Hz, 2H); ^{13}C NMR (101 MHz, $CDCl_3$) δ 148.0, 147.1, 132.5,131.9, 131.5, 129.3, 125.0, 123.5, 122.1, 115.6, 106.7, 92.5, 88.4, 29.6, 18.6, 11.3. ESI-mass (m/z) $[M]^+$: 525; HRMS calculated for $C_{37}H_{40}NSi$ $[M+H]^+$: 526.29245; found: 526.29362.

*2.2.2 Synthesis of 4-((4-ethynylphenyl)ethynyl)-N,N-diphenylaniline (**6**)*

The compound **5** (1.00 g, 1.90 mmol) was dissolved in dry THF (10 mL) and tetra-*n*-butylammonium fluoride (1.10 mL, 3.80 mmol, 0.1 M in THF) was added slowly at room temperature. The reaction was monitored by TLC until all of the starting material disappeared. After evaporation of solvent under reduced pressure, the residue was dissolved in dichloromethane, washed with water followed by brine, and purified by column chromatography (silica gel; hexane: DCM 9:1) to afford titled compound **6** (681 mg, 70%) as an off-white solid; mp: 161–162 °C; FTIR (neat; cm^{-1}): 3442, 2925, 2205, 1587, 1518, 1486, 1316, 1277, 842, 758, 696, 534; ^{1}H NMR (400 MHz, $CDCl_3$) δ 7.44 (s,4H), 7.37 (d, J = 8.8 Hz, 2H), 7.29–7.27 (m, 4H), 7.12 (d, J = 8.6 Hz, 2H), 7.08 (t, J = 7.3 Hz, 2H), 7.01 (d, J = 8.8 Hz, 2H), 3.15 (s, 1H); ^{13}C NMR (101 MHz, $CDCl_3$) δ 148.1, 147.0, 132.5, 132.0, 131.2, 129.3, 125.0, 124.1, 123.6, 122.0, 121.4, 115.5, 91.7, 88.1, 83.3, 78.7; ESI-mass (m/z) $[M+H]^+$: 370; HRMS calculated for $C_{28}H_{20}N$ $[M+H]^+$: 370.15903; found: 370.15971.

*2.2.3 Synthesis of 3-((4-((4-(diphenylamino)phenyl)ethynyl)phenyl)ethynyl)-2H-chromen-2-one (**P1**)*

Compounds **6** (0.50 g, 1.3 mmol) and 3-iodo-2*H*-chromen-2-one (0.375 g, 1.3 mmol) were added to the mixture of *N*,*N*-diisopropylethylamine (5 mL) and dry THF (10 mL) at room temperature. The reaction mixture was subjected to several vacuum/nitrogen cycles and catalytic amounts (ca. 5 mol %) of tetrakis(triphenylphosphine)palladium (0) and copper iodide were added. The reaction mixture was stirred for 30 min at room temperature followed by stirring at 65 °C for 24 h. The solvent was evaporated under reduced pressure and the crude solid was filtered through Celite using dichloromethane. The organic layer was washed with water followed by brine, dried over anhydrous $MgSO_4$ and recovered to get a crude mass which was subjected to column chromatography on silica using DCM: hexane (7: 3) to afford titled target **P1** as a yellow solid (0.49 g, 70%); mp: 209.1–209.9 °C. FTIR (KBr; cm^{-1}): 3038, 2206, 1737, 1588, 1513, 1488, 1286, 1045, 837, 755, 696; ^{1}H NMR (500 MHz, $CDCl_3$) δ 7.95 (s, 1H), 7.55–7.52 (m, 3H), 7.51–7.47 (m, 3H), 7.38–7.35 (m, 3H), 7.32–7.26 (m, 5H), 7.13 (d, J = 9.0 Hz, 4H), 7.07 (t, J = 7.3 Hz, 2H), 7.01 (d, J = 8.8 Hz, 2H); ^{13}C NMR (101 MHz, $CDCl_3$) δ 159.19, 148.17, 147.03, 144.74, 132.57, 132.20, 131.85, 131.34, 129.39, 127.72, 125.07, 123.65, 122.05, 18.88, 116.81, 115.49. 112.96, 95.59, 92.25, 88.26, 84.92; ESI-mass (m/z) $[M+H]^+$ 514; HRMS (APCI): calculated for $C_{37}H_{24}NO_2$ $[M+H]^+$ (m/z) 514.1802; found = 514.1795.

*2.2.4 Synthesis of 2-(4-(diphenylamino)phenyl)-3-(4-((2-oxo-2H-chromen-3-yl)ethynyl)phenyl)buta-1,3-diene-1,1,4,4-tetracarbonitrile (**P2**)*

To a solution of **P1** (100 mg, 0.19 mmol) in dry DCM (10 mL) was added TCNE (74 mg, 0.58 mmol) at room temperature. The reaction mixture was stirred at room temperature for 4 h. The progress of reaction was monitored by TLC. After completion of reaction the solvent was evaporated off and the resulting dark brown mass was purified by column

chromatography (silica gel; hexane: DCM 3: 7) to afford titled **P2** as a brown solid (112 mg, 90%); mp: 196–198 °C; FTIR (KBr; cm^{-1}): 3435, 2854, 2223, 1730, 1586, 1488,1337,756, 700, 528; ^{1}H NMR (500 MHz, $CDCl_3$) δ 8.02 (s, 1H), 7.72 (q, *J* = 8.9 Hz, 4H), 7.65 (d, *J* = 9.3 Hz, 2H), 7.58 (t, *J* = 8.5Hz, 1H), 7.53 (d, *J* = 6.7 Hz, 1H), 7.40 (q, *J* = 7.78 Hz, 4H), 7.30 (dd, *J* = 6.5 Hz, 7.6 Hz, 2H) 7.29 (d, *J* = 7.3Hz, 2H), 7.23 (d, J = 7.4 Hz, 4H), 6.90 (d, *J* = 9.1 Hz, 2H); ^{13}C NMR (125 MHz, $CDCl_3$) δ 167.28, 163.14, 158.85, 153.91, 153.59, 146.21, 144.36, 133.00, 131.83, 130.11, 129.39, 128.04, 126.95, 125.03, 121.00, 118.62, 118.04, 116.94, 113.41, 112.69, 112.11, 111.72, 111.15, 93.74, 88.58, 87.45; ESI-mass (m/z) $[M+H]^+$ 642, HRMS (APCI): calculated for $C_{43}H_{24}N_5O_2$ $[M+H]^+$ (m/z) 642.1925; found = 642.1912.

*2.2.5 Synthesis of 2-(4-(3,3-dicyano-1-(4-(diphenylamino)phenyl)-2-(4-((2-oxo-2H-chromen-3-yl)ethynyl)phenyl)allylidene)cyclohexa-2,5-dien-1-ylidene)malononitrile (**P3**)*

Compounds **P1** (100 mg, 0.19 mmol) and TCNQ (119 mg, 0.58 mmol) were suspended in 1,2- dichlorobenzene and the resulting reaction mixture was stirred at 100 °C for 12 h. The progress of reaction was monitored by TLC. The solvent was evaporated under reduced pressure and the crude residue was purified by column chromatography (silica gel; eluent: DCM) to afford **P3** as a bluish-black solid (97 mg, 70%); mp: 340–342 °C; FTIR (KBr; cm^{-1}): 3038, 2206, 1737, 1588, 1513, 1488, 1455, 1318, 1286, 1045, 837, 755, 696, 530; ^{1}H NMR (400 MHz, $CDCl_3$) δ 8.00 (s, 1H), 7.67–7.49 (m, 7H), 7.39–7.28 (m, 7H), 7.24–7.12 (m, 7H), 7.02–6.99 (d, *J* = 7.6 Hz, 1H), 6.95–6.93 (d, *J* = 8.9 Hz, 2H); ^{13}C NMR (101 MHz, $CDCl_3$) δ 170.92, 159.09, 153.97, 153.73, 151.79, 150.06, 146.18, 145.42, 135.38, 134.53, 134.07, 133.48, 133.43, 133.07, 130.09, 129.76, 128.18, 127.91, 126.77, 126.28, 126.10, 125.21, 119.37, 118.78, 117.12, 114.18, 114.10, 112.81, 112.30, 112.27, 93.98, 88.21, 87.77, 75.18; ESI-mass (m/z) $[M]^+$: 717; HRMS (APCI): calculated for $C_{49}H_{28}N_5O_2$ $[M+H]^+$ (m/z) 718.2238; found = 718.2224. [Note: For experimental spectra, see Supporting Information].

3. Results and discussion

3.1. Optical and electrochemical properties

The optical properties of **P1**, **P2** and **P3** were investigated by measuring their UV–Vis absorption spectra in chloroform solution (Fig. 2) and in pristine as-cast films (Fig. 3). The longest wavelength absorption maximum (λ_{max}) exhibited by **P3** in solution was red-shifted when compared with the solution λ_{max} of **P1** and **P2**. Thin-film spectrum of **P3** indicated better light harvesting properties than either **P2** or **P1**, and an obvious red-shift of ~30 nm remained for **P3**. Two sets of absorption bands (<420 nm and >450 nm) in case of **P2** and **P3** can be assigned to π–π* transition and the intramolecular charge transfer (ICT) transition, respectively, thus indicating that incorporation of additional acceptor units, TCNE and TCNQ, can indeed be utilized for absorbing a larger amount of the solar spectrum. **P3** exhibited a substantial bathochromic shift of the onset absorption wavelength, typically termed as panchromatic absorbance, when compared to **P2**, which is mainly attributed to the presence of the strong electron withdrawing TCNQ unit. Overall, **P2** and **P3** showed better light harvesting properties when compared to **P1** [film λ_{max} of **P1**: 424 nm; **P2**: 431 nm, 523 nm; and **P3**: 345 nm, 661 nm]. According to the spectra shown in Fig. 3, the absorption spectra of **P2** and **P3** complements well with the main absorption of P3HT (380–610 nm), thus indicating that blend films can have more favourable optical absorption throughout the entire visible spectrum and even tailing into the near infrared region. The optical bandgaps estimated from the thin film spectra of **P2** and **P3** were 1.65 eV and 1.34 eV, respectively, which were narrower than the optical band gap of **P1** (= 2.43 eV), an observation that further corroborates the strong accepting capacity of TCNQ given the fact that the other parts, for instance D and A, of the molecular backbone were alike. Thus, the use of the D–A_1–A design

can indeed be helpful for controlling absorption profile, fine tuning energy levels and presumably enhancing BHJ performance.

>Fig. 2<

>Fig. 3<

Theoretical density functional theory (DFT) calculations using the Gaussian 09 suite of programs and the B3LYP/6-311þG(d,p)//B3LYP/6-31G(d) level of theory [45] indicated that the HOMO densities of all the materials were populated over TPA functionality. In case of **P1**, the HOMO density was extended across the central phenyl unit whereas the LUMO density primarily resided over the terminal chromen-2-one functionality. In case of **P2** and **P3**, the LUMO densities were spread along the A_1–A backbone, sparing the phenyl rings of the TPA unit, thus representing an efficient segregation of orbital densities. Such dissociations of theoretical densities can be considered ideal for ICT transition between donor and acceptor fragments. In contrast, the HOMO and LUMO densities of **P1** seem to hold the entire molecular backbone, a result indicating a poor expression of ICT. It is important to point out here that the ester group of chromen-2-one functionality does play a crucial role in tuning the optoelectronic properties of the dyes reported herein. It is apparent from dye **P1** where the LUMO density was completely delocalised on the ester group. Even is case of **P2** and **P3**, it is evident that the ester group does share the LUMO distribution, albeit to a lesser extent. For theoretical density distributions, see Fig. 4 and Section S1 (Supporting Information (SI)). The time-dependant DFT (TD-DFT) calculations further indicated that the dipole moment in the case of **P3** (19.2943 Debye; field-independent basis) was larger than the dipole moments of **P2** (14.0198 Debye) and **P1** (4.2926 Debye), thus indicating an efficient intramolecular charge transfer transition in case of **P3**. Furthermore, the computed

absorption spectra showed the major transition peaks at 465.27 nm, 623.99 nm and 722.25 nm, respectively, for **P1**, **P2** and **P3**. The transition peak in case of **P3** was observed to be red-shifted more than the transition peak of **P2** which in turn was more red-shifted than **P1**, a result that gives support to our experimental finding of optical absorption. For the computed absorption spectra, see Section S2, SI.

>Fig. 4<

As such, the experimental estimation of the HOMO energies was carried out using photo electron spectroscopy in air (PESA) and the LUMO energies were calculated by adding the optical band gap (film spectra) to the HOMO values (for PESA curves see Section S3, SI). The LUMO levels of **P2** and **P3** were deepest when compared with the LUMO level of **P1**. This suggests the influence of additional accepting functionality in tuning the overall energy levels. A similar drop of LUMOs was also observed while conducting DFT calculations (Theoretical LUMOs of **P1**, **P2** and **P3** were -2.72 eV, -3.67 eV and -3.97 eV, respectively), a result that provides a good support to our experimental findings. These theoretical and experimental findings strongly indicate that the D–A_1–A format really plays a crucial role for density segregation, efficient light-harvesting, and tuning optical energy levels when compared with the D–A format. The energy level diagram (Fig. 5) indicated that the band gaps of these materials are all in the range required of acceptor materials for BHJ devices. The electrochemistry experiments revealed that both the compounds **P2** and **P3** undergo reversible reduction processes, thus suggesting their suitability as *n*-type materials in BHJ devices (see Section S4, SI). The HOMO and LUMO levels determined from cyclic-voltammetry experiments were found to be consistent with the energy levels estimated using PESA. We further believed that not only should organic semiconductors be soluble and chemically stable, they should also be thermally stable in order to allow device processing

such as annealing. Keeping this criterion in mind, we conducted thermogravimetric analysis. Thermogravimetric analyses revealed that all the materials are thermally stable chromophores and can endure annealing conditions at a higher temperature, if required (See Section S5 (SI) for TGA curves).

>Fig. 5<

3.2. Photovoltaic properties

Once it was established that new materials displayed promising optoelectronic properties and are potential acceptors with energy levels matching those of the classical electron donor P3HT, solution-processable BHJ devices were fabricated. BHJ architectures typically deliver higher device power conversion efficiencies by maximising the surface area of the interface between *p*- and *n*-type materials in the active layer. The BHJ device architecture used was indium-tin oxide (ITO)/poly(3,4-ethylenedioxythiophene): polystyrene sulfonate (PEDOT:PSS, 38 nm)/active layer (~60 nm)/Ca (20 nm)/Al (100 nm) where the active layer was a 1: 1 blend of P3HT: **P1**/**P2**/**P3**, respectively, spin-cast from *o*-dichlorobenzene on top of the PEDOT: PSS surface. It is apparent that we chose a simple device architecture to observe initial performance and fabricating conditions of BHJ devices. Control devices based on P3HT: $PC_{61}BM$ were also fabricated. A promising and high PCE of 4.21% was achieved when P3HT: **P3** blend film (1: 1) was spin-coated from *o*-chlorobenzene solution. By contrast, the maximum PCEs obtained from the devices based on **P2** and **P1** were 3.75% and 2.28%, respectively, when fabricated under similar conditions.

We used *o*-dichlorobenzene as the processing solvent as the use of high boiling solvent is preferred for optimal performance and to avoid formation of large-scale crystals on active surfaces. The optimized donor: acceptor weight ratio was found to be 1: 1 where the BHJ devices gave encouraging performance. Other donor: acceptor combinations, for example 1:

2 (**P2** and **P3**), afforded poor device outcome, thus indicating that 1: 1 blend is optimum for the current study of P3HT and non-fullerene acceptors. We realized that this inferior performance (1: 2 combination) may be attributed to low film quality where we physically observed roughness on active surfaces. The PCE of **P3**-based devices (donor/acceptor 1: 1) is higher than that of its counterparts, **P2** and **P1**, primarily in terms of the enhanced short circuit current density (J_{sc}), which might be attributed to the broader absorption profile of **P3** which in fact can facilitate the harvesting of more solar photons. The **P2**-based devices afforded reasonable outcome too, almost two-fold efficiency when compared with **P1**-based devices, thus indicating that the incorporation of an additional acceptor functionality, for instance TCNE or TCNQ in the present study, in a given D–A system is advantageous not only for tuning optoelectronic properties but for device outcome too. This validates the use of D–A_1–A modular format as a favourable structural concept for the design and development of efficient non-fullerene acceptors when compared with the D–A format. The maximum PCE reached 3.08% for a device based on P3HT:$PC_{61}BM$ when fabricated under similar conditions. For current–voltage (*J*–*V*) curves see Fig. 6 and Table S1 (SI) represents comparative photovoltaic data.

>Fig. 6<

The incident photon to current conversion efficiency (IPCE) curves of the best BHJ devices based on **P2** and **P3** under monochromatic light are shown in Fig. 7. For **P2**, the IPCE shows a maximum of ~46% at 510 nm whereas for **P3**, the IPCE spectrum shows a much broader response covering most of the visible region (400–800 nm) and to the near IR region with a maximum value of ~60% at 700 nm. The IPCE spectra of the devices closely resemble the blend film spectra of corresponding active layers (Fig. 7), thus demonstrating that both donor

and acceptor domains contributed to the photocurrent generation. Better BHJ performance and the higher peak IPCE in case of **P3** can be held responsible by the synergetic effect of better light-harvesting and the use of stronger TCNQ derived acceptor when compared with **P2** reported herein. The **P1**-based device afforded poor IPCE characteristics to be reported. The broadness of these IPCE spectra, **P3** in particular, indicates these non-fullerene acceptors can definitely be matched with a variety of electron donors, such as conjugated polymers and small molecules, in order to achieve charge generation over a broad range of wavelengths.

>Fig. 7<

The physical microstructure of the blend surfaces was examined using atomic force microscopy (AFM) in tapping mode. Fig. 8 displays the topographic and phase images of 1:1 blends of **P2** and **P3** with P3HT (1:1 *w*/*w*). **P2** appears to have a granular morphology with surface roughness of ~3.7 nm, whereas blend film of **P3** appears to be smooth with better phase separation and with a root-mean square (RMS) roughness of 1.2 nm. It is apparent that both the materials blended well with their donor counterpart and that the superior morphological properties of **P3**-based blend have had a greater effect on efficiency when compared with the **P2**-based blend. Superiority of **P3**-based blend surface was also confirmed by the transmission electron microscopy (TEM) analysis where we were able to observe a finer texture, a finding that usually results in relatively higher values of J_{sc} and FF, when compared with the **P2**-based blend (Fig. 9). It was also evident that the AFM analyses supported our physical observation of the blend surfaces. To gain an insight into the effective charge carrier mobilities, the space charge limited current (SCLC) method was applied to get information about the charge transportation in the devices. The electron-only devices, consisting of active layer sandwiched between a ZnO coated ITO electrode and LiF/Al

counter-electrode as the hole-blocking contact, were fabricated as per the sketch depicted in Section S6, SI. From the current density as a function of voltage data (Section S6 (SI)), the electron mobility in the trap-free SCLC region can be estimated using the Mott-Gurney equation, [($J = 9\ (\varepsilon\mu)/8 \times (V^2/d^3)$); where ε is the dielectric constant, μ is the charge-carrier mobility, d is the sample thickness, and V is the applied voltage]. Using this expression, the electron mobilities of the order of 10^{-4} cm^2/Vs were observed for both **P2** and **P3**. It is vital to point out that the mobilities of the obtained order are well within the mobility range exhibited by $PC_{61}BM$ (typically ranging 10^{-3}–10^{-4} $cm^2\ V^{-1}\ s^{-1}$). Evidently, the observance of good electron mobility further supports the design principle of these new materials.

>Fig. 8<

>Fig. 9<

It is judicious to mention that though the PCE numbers steadily improve with the use of non-fullerene acceptors combined with high performing donor polymers and small molecular solids, we believe in continued emphasis on systematic material design and developing those non-fullerene acceptors which can interweave well with the commercially available donors, such as P3HT, hence demonstrating their foremost suitability to be an efficient acceptor. Having said this, and taking into account the D–A_1–A-based acceptors reported in the literature, it is justifiable to say that the device outcome reported herein provides strong support and incentive for the current research strategy.

4. Conclusions

We have been able to demonstrate the successful use of a D–A_1–A modular format in BHJ solar cells. The new materials **P2** and **P3** were designed and synthesized based on the D–A_1–

A format and their optoelectronic and photovoltaic properties were directly compared with a structural analogue **P1**, which was based on a simple D–A modular design. It was observed that **P2** and **P3** exhibited superior properties, such as light-harvesting, enhanced photocurrent density and overall device performance, when compared with **P1**. Overall, **P3** performed better than any of the three materials reported herein. It is notable to mention that not only are **P1**, **P2** and **P3** the first examples in the literature which comprise promising building blocks, such as TPA and terminal chromen-2-one, but the device parameters outlined herein are among the highest numbers reported in this class of materials.

Acknowledgments

S. V. B. (RMIT) acknowledges financial support from the Australian Research Council (ARC), Australia, under a Future Fellowship Scheme (FT110100152). A. G. is thankful to the Alfred Deakin Fellowship Scheme at the IFM, Deakin University, Waurn Ponds Victoria Australia. We also acknowledge Duong Duc La for TEM measurements. The CSIRO Division of Manufacturing, Clayton Victoria, Australia is acknowledged for providing support through a visiting fellow position for A. G. A. G. acknowledges a vast variety of facilities at Deakin University, RMIT University and Bio 21 Institute, the University of Melbourne, Melbourne Victoria Australia. S. V. B. (IICT) would like to thank the TAPSUN programme for financial assistance under the project NWP0054. P. S. R. acknowledges to CSIR, New Delhi for senior research fellowship (SRF).

References

[1] Becquerel A. Recherches sur les effets de la radiation chimique de la lumiere solaire au moyen des courants electriques. C R Acad Sci 1839;9:145–9.

[2] Tang CW. Two-layer organic photovoltaic cell. Appl Phys Lett 1986;48(2):183–5

[3] Yu G, Gao J, Hummelen JC, Wudl F, Heeger AJ. Polymer photovoltiac cells: Enhanced efficiencies via a network of internal donor-acceptor heterojunctions. Science 1995;270(5243):1789.

[4] Xiang W, Gupta A, Kashif MK, Duffy N, Bilic A, Evans RA, et al. Cyanomethylbenzoic Acid: An Acceptor for Donor–π–Acceptor Chromophores Used in Dye-Sensitized Solar Cells. ChemSusChem 2013;6(2):256–60.

[5] Heeger AJ. 25th anniversary article: bulk heterojunction solar cells: understanding the mechanism of operation. Adv Mater 2014;26(1):10–28.

[6] Huang Y, Kramer EJ, Heeger AJ, Bazan GC. Bulk heterojunction solar cells: morphology and performance relationships. Chem Rev 2014;114(14):7006–43.

[7] Lin Y, Li Y, Zhan X. Small molecule semiconductors for high-efficiency organic photovoltaics. Chem Soc Rev 2012;41(11):4245–72.

[8] You J, Dou L, Yoshimura K, Kato T, Ohya K, Moriarty T, et al. A polymer tandem solar cell with 10.6% power conversion efficiency. Nat Commun 2013;4:1446.

[9] Chen JD, Cui C, Li YQ, Zhou L, Ou QD, Li C, et al. Single-junction polymer solar cells exceeding 10% power conversion efficiency. Adv Mater 2015;27(6):1035–41.

[10] Kan B, Li M, Zhang Q, Liu F, Wan X, Wang Y, et al. A series of simple oligomer-like small molecules based on oligothiophenes for solution-processed solar cells with high efficiency. J Am Chem Soc 2015;137(11):3886–93.

[11] Zhong Y, Trinh MT, Chen R, Wang W, Khlyabich PP, Kumar B, et al. Efficient organic solar cells with helical perylene diimide electron acceptors. J Am Chem Soc 2014;136(43):15215–21.

[12] Li H, Hwang YJ, Courtright BA, Eberle FN, Subramaniyan S, Jenekhe SA. Fine-tuning the 3D structure of nonfullerene electron acceptors toward high-performance polymer solar cells. Adv Mater 2015;27(21):3266–72.

[13] Shin RY, Sonar P, Siew PS, Chen Z-K, Sellinger A. Electron-accepting conjugated materials based on 2-vinyl-4, 5-dicyanoimidazoles for application in organic electronics. J Org Chem 2009;74(9):3293–8.

[14] Zhao W, Qian D, Zhang S, Li S, Inganäs O, Gao F, et al. Fullerene-free polymer solar cells with over 11% efficiency and excellent thermal stability. Adv Mater 2016;28(23):4734–9.

[15] Li S, Ye L, Zhao W, Zhang S, Mukherjee S, Ade H, et al. Energy-level modulation of small-molecule electron acceptors to achieve over 12% efficiency in polymer solar cells. Adv Mater 2016;28(42):9423–9.

[16] Lin Y, Zhang Z-G, Bai H, Wang J, Yao Y, Li Y, et al. High-performance fullerene-free polymer solar cells with 6.31% efficiency. Energy Environ Sci 2015;8(2):610–6.

[17] Lin Y, Wang J, Zhang ZG, Bai H, Li Y, Zhu D, et al. An electron acceptor challenging fullerenes for efficient polymer solar cells. Adv Mater 2015;27(7):1170–4.

[18] Liu X, Xie Y, Zhao H, Cai X, Wu H, Su S-J, et al. Star-shaped isoindigo-based small molecules as potential non-fullerene acceptors in bulk heterojunction solar cells. New J Chem 2015;39(11):8771–9.

[19] Liu X, Luo G, Cai X, Wu H, Su S-J, Cao Y. Pyrene terminal functionalized perylene diimide as non-fullerene acceptors for bulk heterojunction solar cells. RSC Adv 2015;5(101):83155–63.

[20] Liu X, Xie Y, Cai X, Li Y, Wu H, Su S-J, et al. Synthesis and photovoltaic properties of A–D–A type non-fullerene acceptors containing isoindigo terminal units. RSC Adv 2015;5(130):107566–74.

[21] Hwang YJ, Li H, Courtright BA, Subramaniyan S, Jenekhe SA. Nonfullerene polymer solar cells with 8.5% efficiency enabled by a new highly twisted electron acceptor dimer. Adv Mater 2016;28(1):124–31.

[22] Wen D, Yue F, Li G, Zheng G, Chan K, Chen S, et al. Helicity multiplexed broadband metasurface holograms. Nat Commun 2015;6(8241).

[23] Li S, Liu W, Shi M, Mai J, Lau T-K, Wan J, et al. A spirobifluorene and diketopyrrolopyrrole moieties based non-fullerene acceptor for efficient and thermally stable polymer solar cells with high open-circuit voltage. Energy Environ Sci 2016;9(2):604–10.

[24] Patil H, Zu WX, Gupta A, Chellappan V, Bilic A, Sonar P, et al. A non-fullerene electron acceptor based on fluorene and diketopyrrolopyrrole building blocks for solution-processable organic solar cells with an impressive open-circuit voltage. Phys Chem Chem Phys 2014;16(43):23837–42.

[25] Raynor AM, Gupta A, Patil H, Bilic A, Bhosale SV. A diketopyrrolopyrrole and benzothiadiazole based small molecule electron acceptor: design, synthesis, characterization and photovoltaic properties. RSC Adv 2014;4(101):57635–8.

[26] Patil H, Gupta A, Alford B, Ma D, Privér SH, Bilic A, et al. Conjoint use of dibenzosilole and indan-1, 3-dione functionalities to prepare an efficient non-fullerene acceptor for solution-processable bulk□heterojunction solar cells. Asian J Org Chem 2015;4(10):1096–102.

[27] Gupta A, Rananaware A, Rao PS, La DD, Bilic A, Xiang W, Li J, Evans RA, Bhosale SV, Bhosale SV. An H-shaped, small molecular non-fullerene acceptor for efficient organic solar cells with an impressive open-circuit voltage of 1.17 V. Mater Chem Front 2017;DOI: 10.1039/C7QM00084G

[28] Srivani D, Gupta A, La DD, Bhosale RS, Puyad AL, Xiang W, Li J, Bhosale SV, Bhosale SV. Small molecular non-fullerene acceptors based on naphthalenediimide and benzoisoquinoline-dione functionalities for efficient bulk-heterojunction devices. Dyes Pigm 2017;143:1–9

[29] Srivani D, Gupta A, Bhosale SV, Puyad AL, Xiang W, Li J, Evans RA, Bhosale SV. Non-fullerene acceptors based on central naphthalene diimide flanked by rhodanine or 1,3-indanedione. Chem Commun 2017;53:7080–7083.

[30] Chen W, Zhang Q. Recent progress in non-fullerene small molecule acceptors in organic solar cells. J Mater Chem C 2017;5:1275–1302.

[31] Chen W, Yang X, Long G, Wan X, Chen Y, Zhang Q. A perylene diimide (PDI)-based small molecule with tetrahedral configuration as a non-fullerene acceptor for organic solar cells. J Mater Chem C 2015;3:4698–4705.

[32] Hu B, Li M, Chen W, Wan X, Chen Y, Zhang Q. Novel donor–acceptor polymers based on 7-perfluorophenyl-6*H*-[1,2,5]thiadiazole[3,4-*g*]benzoimidazole for bulk heterojunction solar cells. RSC Adv 2015;5:50137–50145.

[33] Chen W, Salim T, Fan H, James L, Lam YM, Zhang Q. Quinoxaline-functionalized C_{60} derivatives as electron acceptors in organic solar cells. RSC Adv 2014;4:25291–2530.

[34] Chen W, Zhang Q, Salim T, Ekahana SA, Wan X, Sum TC, et al. Synthesis and photovoltaic properties of novel C_{60} bisadducts based on benzo[2,1,3]-thiadiazole. Tetrahedron 2014;70:6217–6221.

[35] Leu WC, Hartley CS. A push–pull macrocycle with both linearly conjugated and cross-conjugated bridges. Org Lett 2013;15(14):3762–5.

[36] Gholami M, Tykwinski RR. Oligomeric and polymeric systems with a cross-conjugated π-framework. Chem Rev 2006;106(12):4997–5027.

[37] Zucchero AJ, McGrier PL, Bunz UH. Cross-conjugated cruciform fluorophores. Acc Chem Res 2009;43(3):397–408.

[38] Gupta A, Ali A, Bilic A, Gao M, Hegedus K, Singh B, et al. Absorption enhancement of oligothiophene dyes through the use of a cyanopyridone acceptor group in solution-processed organic solar cells. Chem Commun 2012;48(13):1889–91.

[39] Gupta A, Armel V, Xiang W, Fanchini G, Watkins SE, MacFarlane DR, et al. The effect of direct amine substituted push–pull oligothiophene chromophores on dye-sensitized and bulk heterojunction solar cells performance. Tetrahedron 2013;69(17):3584–92.

[40] Kumar RJ, Churches QI, Subbiah J, Gupta A, Ali A, Evans RA, et al. Enhanced photovoltaic efficiency via light-triggered self-assembly. Chem Commun 2013;49(58):6552–4.

[41] Gupta A, Ali A, Singh TB, Bilic A, Bach U, Evans RA. Molecular engineering for panchromatic absorbing oligothiophene donor–π–acceptor organic semiconductors. Tetrahedron 2012;68(46):9440–7.

[42] Raynor AM, Gupta A, Patil H, Ma D, Bilic A, Rook TJ, et al. A non-fullerene electron acceptor based on central carbazole and terminal diketopyrrolopyrrole functionalities for efficient, reproducible and solution-processable bulk-heterojunction devices. RSC Adv 2016;6(33):28103–9.

[43] Florian A, Mayoral MJ, Stepanenko V, Fernández G. Alternated stacks of nonpolar oligo (p-phenyleneethynylene)-BODIPY systems. Chem Eur J 2012;18(47):14957–61.

[44] Schmittel M, Ammon H. Preparation of a rigid macrocycle with two exotopic phenanthroline binding sites Synlett 1999;6(06):750–2.

[45] Frisch M, Trucks G, Schlegel H, Scuseria G, Robb M, Cheeseman J, et al. Gaussian 09, Revision D. 01. Wallingford CT: Gaussian Inc.; 2013.

Figure and Scheme Captions

Fig. 1. Molecular structures of the newly designed and synthesized non-fullerene electron acceptors, **P1**, **P2** and **P3**.

Scheme 1. Synthetic protocol adopted to synthesize **P1**; Reagents and conditions**: I**) trimethylsilylacetylene (TMSA), $Pd(PPh_3)_2Cl_2$/CuI, Et_3N, RT, 20 h, 98%; **II**) (triisopropylsilyl)acetylene (TIPS), $Pd(PPh_3)_2Cl_2$/CuI, Et_3N, 4 days, reflux, 97%; **III**) K_2CO_3, THF: MeOH (1: 1), RT, 4 h, 82%; **IV**) $Pd(PPh_3)_2Cl_2$/CuI, *N*,*N*-diisopropylethylamine (DIPEA), dry Toluene, RT, 12 h, 91%; **V**) tetra-n-butylammonium fluoride $[C_4H_9)_4NF]$, dry THF, RT, 1 h, 70%; **VI**) $Pd(PPh_3)_4$/CuI, DIPEA, dry THF, 65 ºC, 24 h.

Scheme 2. Synthesis of compounds **P2** and **P3**.

Fig. 2. Absorption spectra of compounds **P1**, **P2** and **P3** in their chloroform solutions (equimolar solutions of 10 µM concentration).

Fig. 3. Absorption spectra of compounds **P1**, **P2** and **P3** for pristine as-cast films (films were spin-casted at 2500 rpm for 1 min to give a film thickness of ~ 65 nm).

Fig. 4. Theoretical density distribution for the HOMOs (left) and LUMOs (right) of **P1**, **P2** and **P3**.

Fig. 5. Energy level diagram showing alignments of different components of BHJ device architecture.

Fig. 6. Characteristic current-density *vs* voltage (*J*-*V*) curves for the best BHJ devices based on **P1**/**P2**/**P3** in blends with P3HT under simulated sunlight (100 mW cm^{-2} AM1.5G). Device structure is: ITO/PEDOT: PSS (38 nm)/active layer/Ca (20 nm)/Al (100 nm). The active layer thicknesses were in the range of 60–65 nm with *w*: *w* = 1: 1.

Fig. 7. IPCE spectra of the best performing devices described in Fig. 6.

Fig. 8. AFM images of 1: 1 blend films with P3HT spin-cast from *o*-chlorobenzene at 2500 rpm atop annealed ITO/PEDOT: PSS substrates. Topographic (left) and phase images (right) for P3HT: **P2** (upper) and P3HT: **P3** (lower) are depicted.

Fig 9. TEM images for 1: 1 blend of P3HT: **P2** (left) and P3HT: **P3** (right) showing superior mixing of donor and acceptor domains in case of **P3** when compared with **P2**-based blend. Scale bar of 50 nm is represented.

Figures and Schemes

Fig. 1

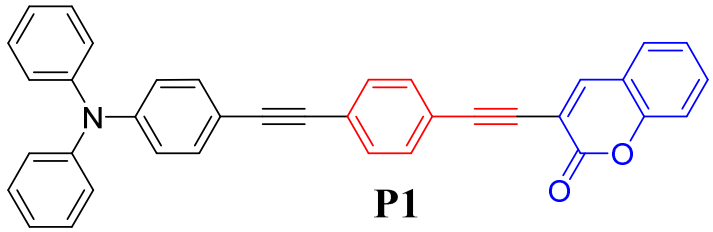

P1

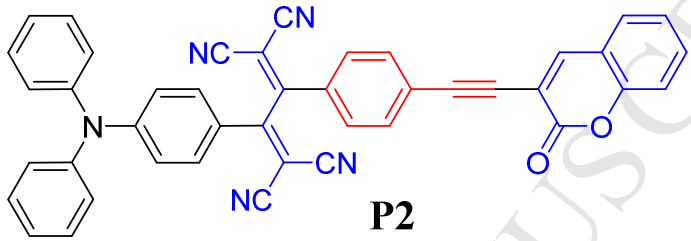

P2

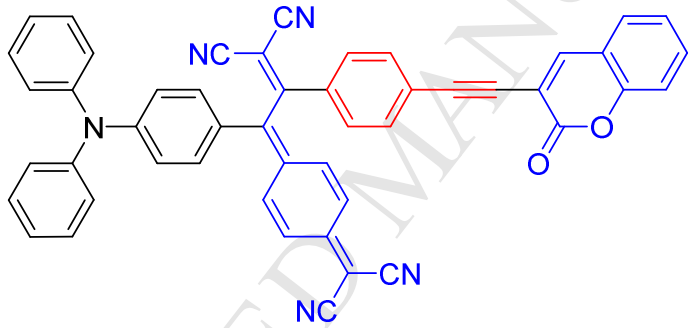

P3

Scheme 1

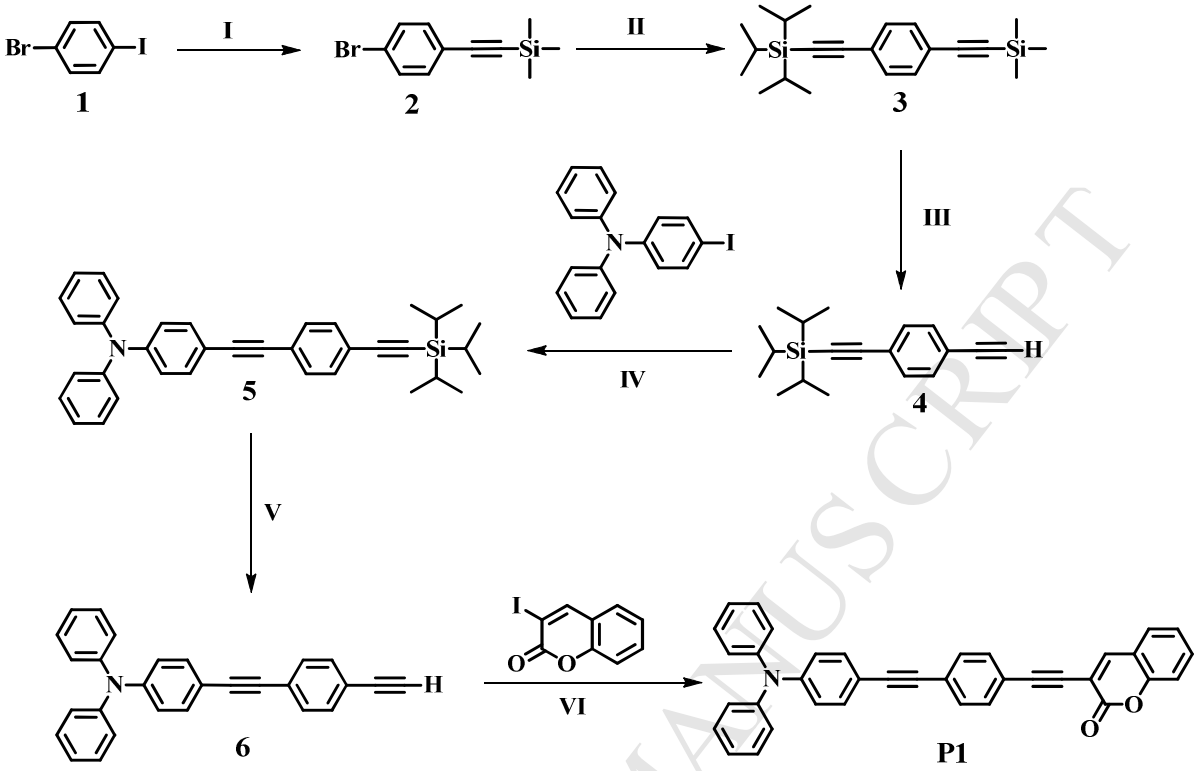

Scheme 2

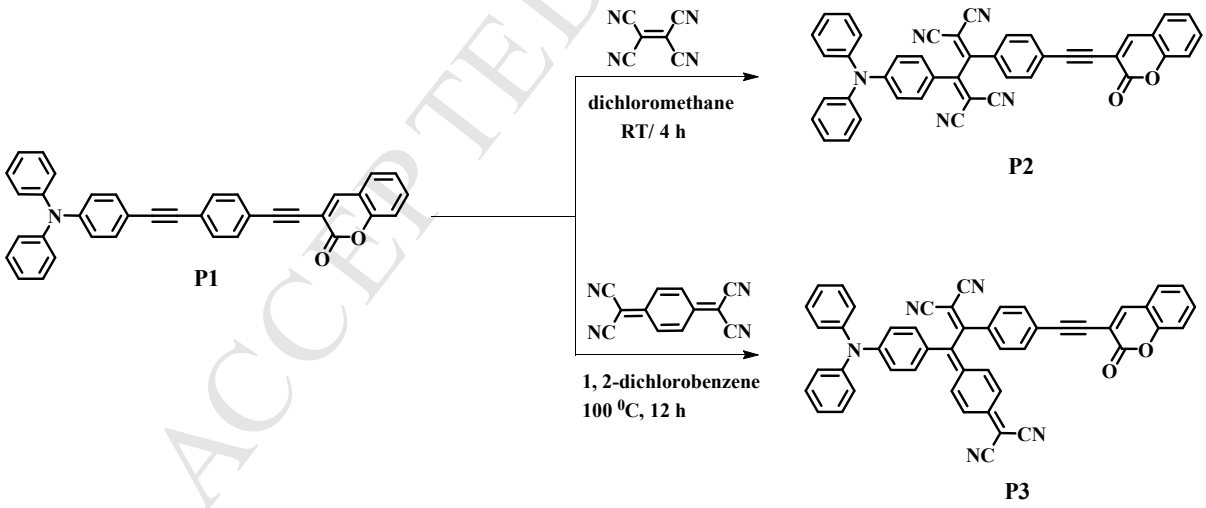

Fig. 2

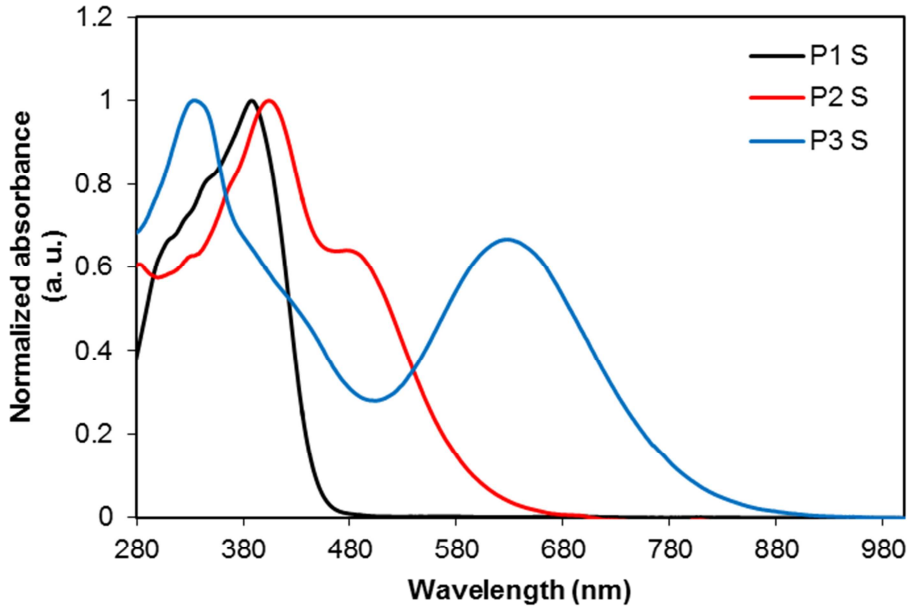
1.2
1
0.8
0.6
0.4
0.2
0
Normalized absorbance (a. u.)
280
380
480
580
680
780
880
980
Wavelength (nm)
P1 S
P2 S
P3 S

Fig. 3

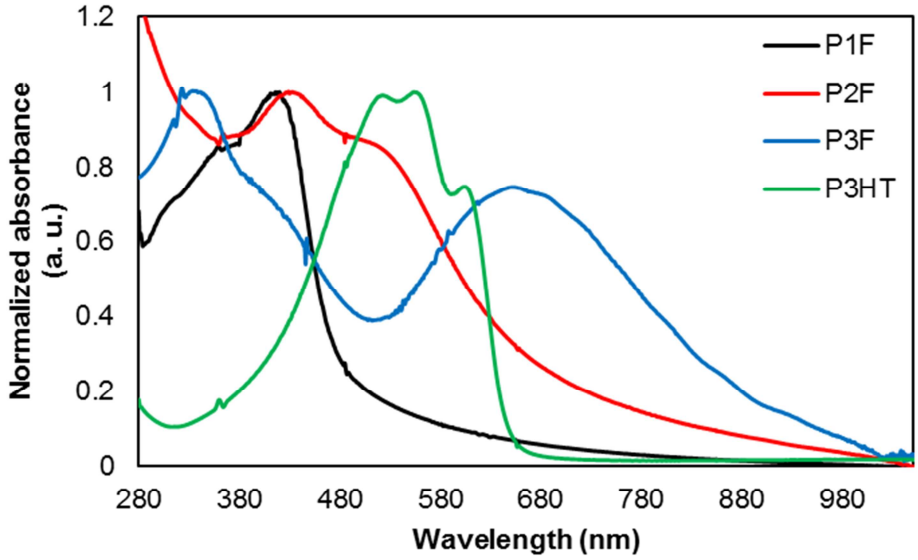
1.2
1
0.8
0.6
0.4
0.2
0
Normalized absorbance (a. u.)
280
380
480
580
680
780
880
980
Wavelength (nm)
P1F
P2F
P3F
P3HT

Fig. 4

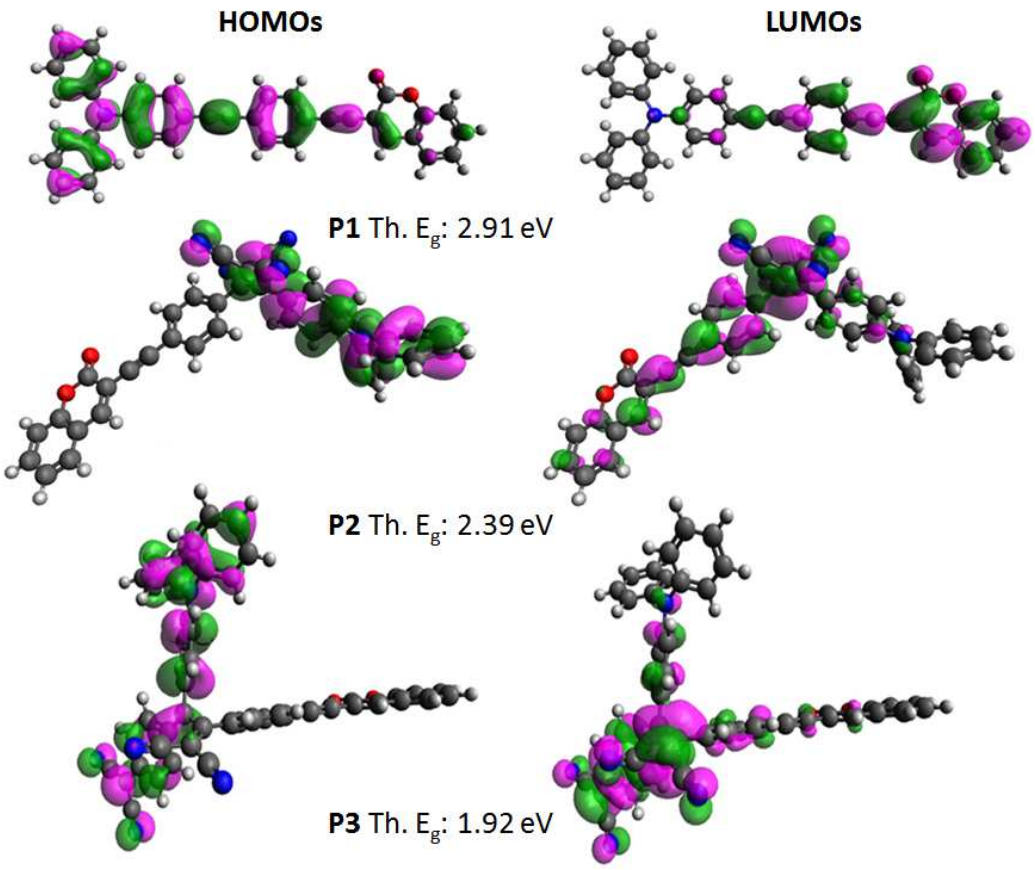

Fig. 5

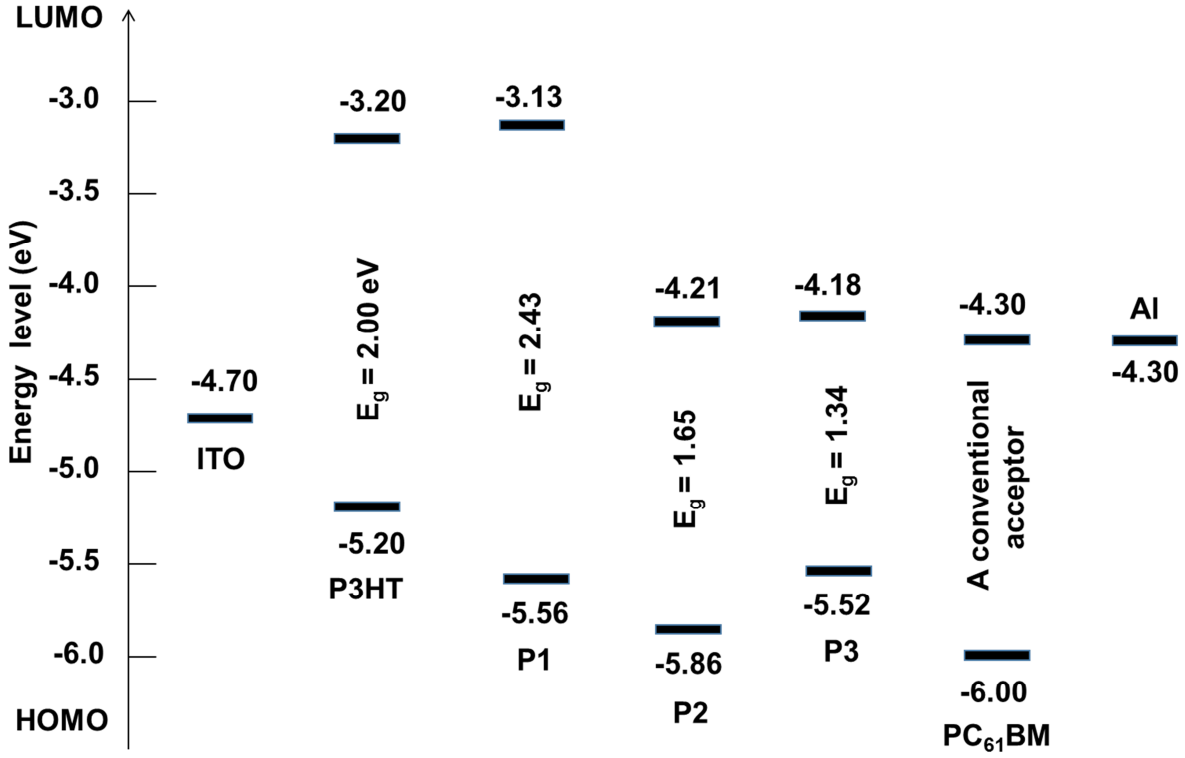
LUMO
HOMO
Energy level (eV)
-3.0
-3.5
-4.0
-4.5
-5.0
-5.5
-6.0
-4.70
ITO
-3.20
-5.20
P3HT
Eg = 2.00 eV
-3.13
-5.56
P1
Eg = 2.43
-4.21
-5.86
P2
Eg = 1.65
-4.18
-5.52
P3
Eg = 1.34
-4.30
-6.00
PC61BM
A conventional acceptor
Al
-4.30

Fig. 6

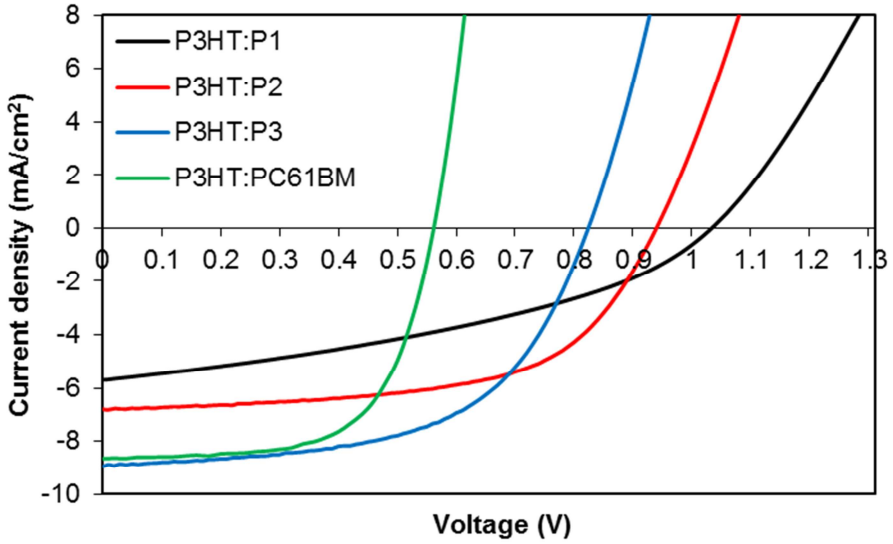
P3HT:P1
P3HT:P2
P3HT:P3
P3HT:PC61BM
Current density (mA/cm2)
Voltage (V)
8
6
4
2
0
-2
-4
-6
-8
-10
0
0.1
0.2
0.3
0.4
0.5
0.6
0.7
0.8
0.9
1
1.1
1.2
1.3

Fig. 7

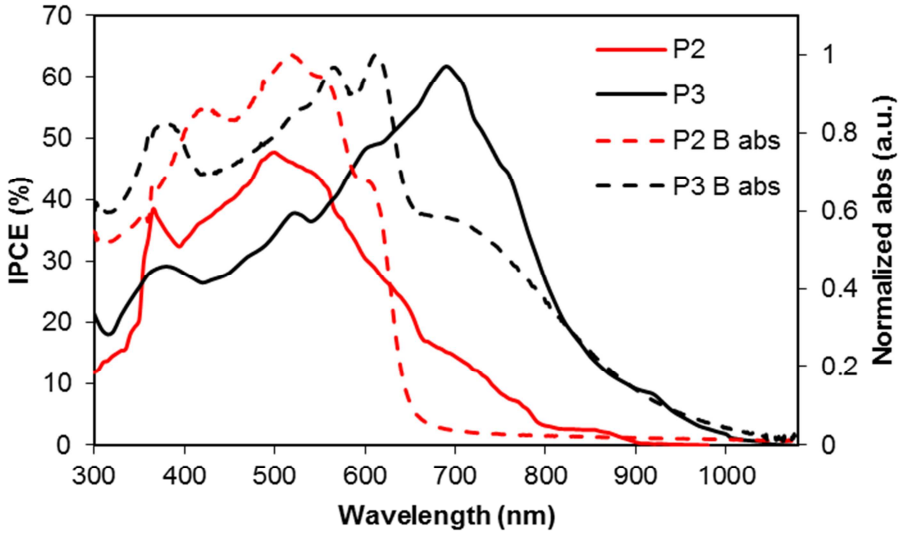

Fig. 8

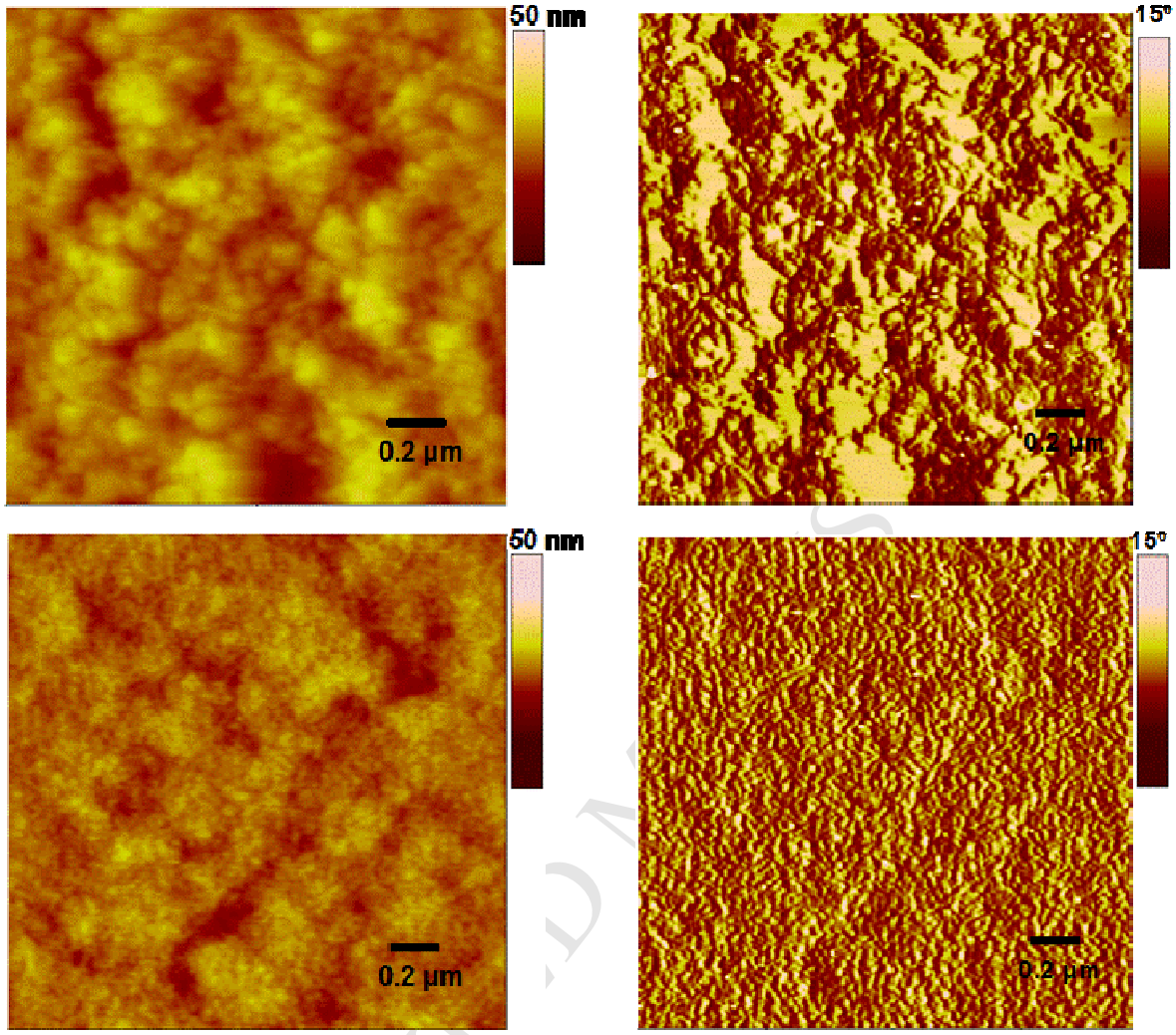

Fig. 9

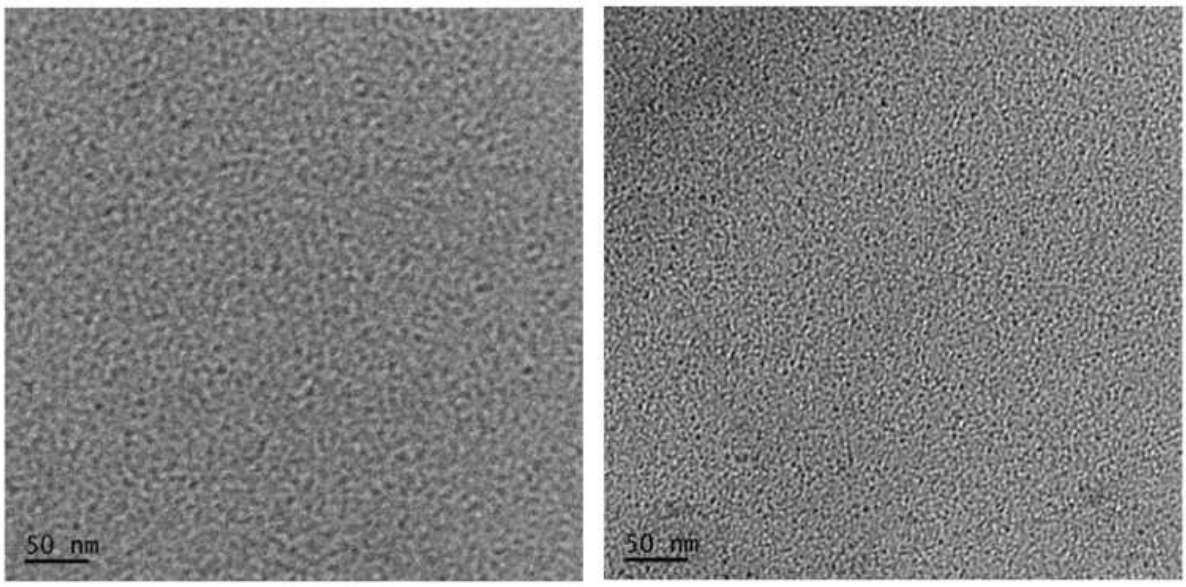

Supporting Information

Donor–acceptor–acceptor-based non-fullerene acceptors comprising terminal chromen-2-one functionality for efficient bulk-heterojunction devices

Pedada Srinivasa Rao,[a,b] Akhil Gupta,*[c] Sidhanath V. Bhosale,*[a] Ante Bilic,[d] Wanchun Xiang,[e] Richard A. Evans[f] and Sheshanath V. Bhosale*[g]

a Polymers and Functional Materials Division, CSIR-Indian Institute of Chemical Technology, Hyderabad 500007, Telangana, India; Email: bhosale@iict.res.in

b Academy of Scientific and Innovative Research (AcSIR), CSIR-IICT, Hyderabad 500007, Telangana, India

c Institute for Frontier Materials, Deakin University, Waurn Ponds, Victoria 3216 Australia; Tel: +61 3 5247 9542; E-mail: akhil.gupta@deakin.edu.au

d Data61 CSIRO, Molecular and Materials Modelling, Docklands, Victoria 8012 Australia

e State Key Laboratory of Silicate Materials for Architectures, Wuhan University of Technology, 122 Luoshi Rd, Wuhan 430070 Hubei, P. R. China

f CSIRO Manufacturing, Bayview Avenue, Clayton South, Victoria 3169 Australia

g School of Science, RMIT University, GPO Box 2476, Melbourne Victoria 3001 Australia; Tel: +61 3 9925 2680; E-mail: sheshanath.bhosale@rmit.edu.au

Section S1

Theoretical density distribution for various energy states:

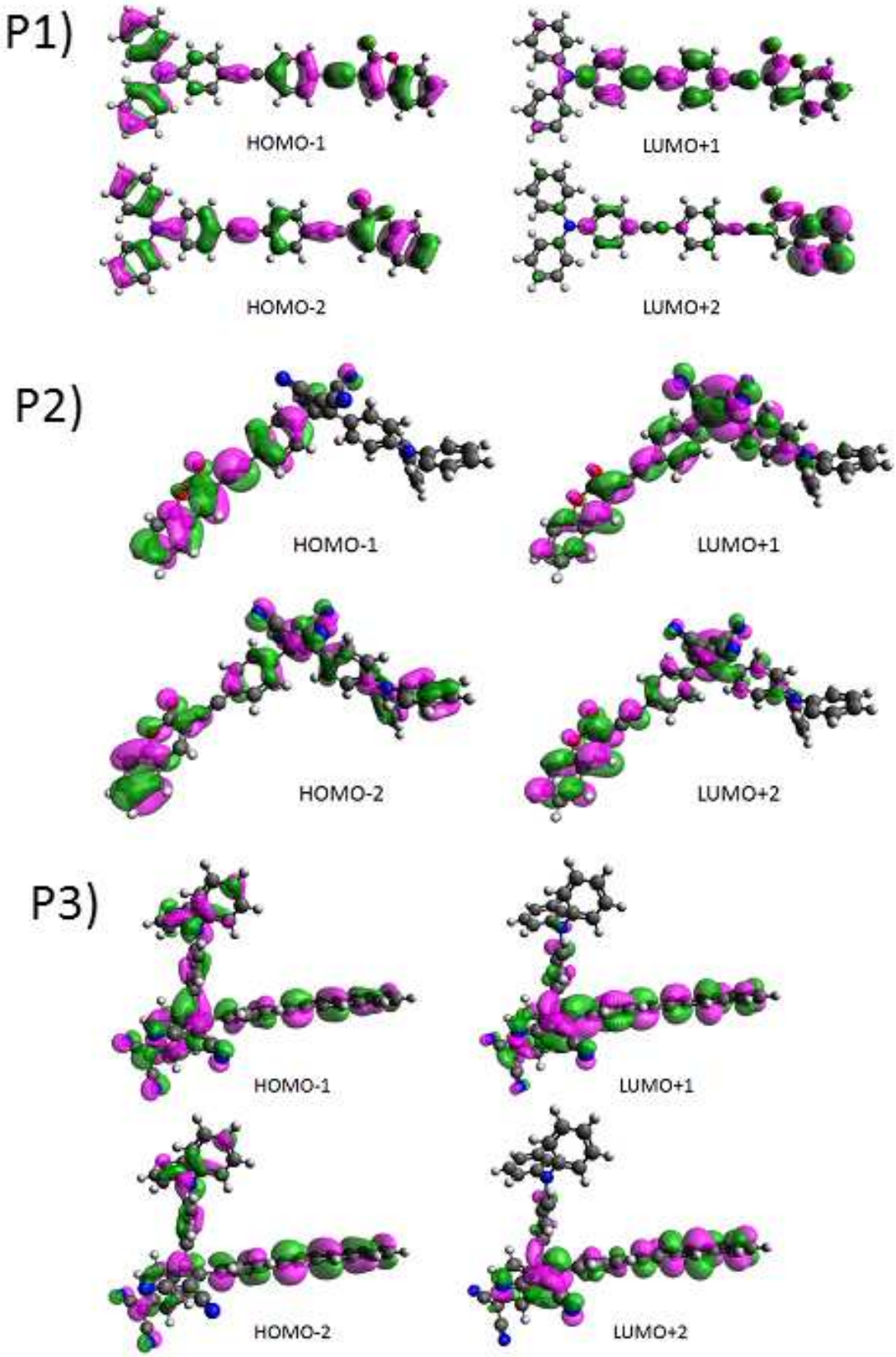

Tabular form of energy levels of theoretical density distributions:

Dye	HOMO (eV)	LUMO (eV)	HOMO-1 (eV)	LUMO+1 (eV)	HOMO-2 (eV)	LUMO+2 (eV)
P1	-5.63	-2.72	-6.19	-1.81	-6.85	-0.98
P2	-6.06	-3.67	-6.55	-3.13	-7.37	-2.65
P3	-5.89	-3.97	-6.61	-3.38	-6.70	-2.75

Section S2

Time-dependant DFT (TD-DFT) calculations depicting calculated dipole moments and optical absorption curves:

P1:

Excited	State	1:	Singlet-A'	2.6648	eV	465.27	nm	f=1.3690	<S**2>=0.000
Excited	State	2:	Singlet-A'	3.2374	eV	382.97	nm	f=0.8541	<S**2>=0.000
Excited	State	3:	Singlet-A'	3.4944	eV	354.81	nm	f=0.4786	<S**2>=0.000
Excited	State	4:	Singlet-A'	3.7910	eV	327.05	nm	f=0.0068	<S**2>=0.000
Excited	State	5:	Singlet-A'	3.9912	eV	310.65	nm	f=0.0137	<S**2>=0.000
Excited	State	6:	Singlet-A'	4.1087	eV	301.76	nm	f=0.0001	<S**2>=0.000
Excited	State	7:	Singlet-A'	4.1152	eV	301.29	nm	f=0.0248	<S**2>=0.000
Excited	State	8:	Singlet-A"	4.1319	eV	300.07	nm	f=0.0000	<S**2>=0.000
Excited	State	9:	Singlet-A'	4.1432	eV	299.25	nm	f=0.0002	<S**2>=0.000
Excited	State	10:	Singlet-A'	4.2157	eV	294.10	nm	f=0.0037	<S**2>=0.000

P2:

Excited	State	1:	Singlet-A	1.9870	eV	623.99	nm	f=0.0852	<S**2>=0.000
Excited	State	2:	Singlet-A	2.5734	eV	481.79	nm	f=0.7053	<S**2>=0.000
Excited	State	3:	Singlet-A	2.6877	eV	461.31	nm	f=0.4055	<S**2>=0.000
Excited	State	4:	Singlet-A	3.0446	eV	407.23	nm	f=0.6979	<S**2>=0.000
Excited	State	5:	Singlet-A	3.1073	eV	399.01	nm	f=0.0788	<S**2>=0.000
Excited	State	6:	Singlet-A	3.3090	eV	374.69	nm	f=0.0908	<S**2>=0.000
Excited	State	7:	Singlet-A	3.4090	eV	363.70	nm	f=0.1264	<S**2>=0.000
Excited	State	8:	Singlet-A	3.5242	eV	351.81	nm	f=0.0022	<S**2>=0.000
Excited	State	9:	Singlet-A	3.5542	eV	348.84	nm	f=0.0827	<S**2>=0.000
Excited	State	10:	Singlet-A	3.6124	eV	343.21	nm	f=0.0052	<S**2>=0.000
Excited	State	11:	Singlet-A	3.6583	eV	338.91	nm	f=0.0207	<S**2>=0.000
Excited	State	12:	Singlet-A	3.7703	eV	328.85	nm	f=0.0214	<S**2>=0.000
Excited	State	13:	Singlet-A	3.8041	eV	325.93	nm	f=0.0041	<S**2>=0.000
Excited	State	14:	Singlet-A	3.8085	eV	325.55	nm	f=0.0118	<S**2>=0.000

P3:

Excited	State	1:	Singlet-A	1.7166	eV	722.25	nm	f=0.2899	<S**2>=0.000
Excited	State	2:	Singlet-A	2.1929	eV	565.39	nm	f=0.3234	<S**2>=0.000
Excited	State	3:	Singlet-A	2.3614	eV	525.04	nm	f=0.1299	<S**2>=0.000
Excited	State	4:	Singlet-A	2.5073	eV	494.50	nm	f=0.4856	<S**2>=0.000
Excited	State	5:	Singlet-A	2.8241	eV	439.02	nm	f=0.1038	<S**2>=0.000
Excited	State	6:	Singlet-A	2.8951	eV	428.25	nm	f=1.0828	<S**2>=0.000
Excited	State	7:	Singlet-A	3.0681	eV	404.11	nm	f=0.2847	<S**2>=0.000
Excited	State	8:	Singlet-A	3.2353	eV	383.23	nm	f=0.0603	<S**2>=0.000
Excited	State	9:	Singlet-A	3.2898	eV	376.88	nm	f=0.0258	<S**2>=0.000
Excited	State	10:	Singlet-A	3.3141	eV	374.11	nm	f=0.0097	<S**2>=0.000
Excited	State	11:	Singlet-A	3.4425	eV	360.16	nm	f=0.0031	<S**2>=0.000
Excited	State	12:	Singlet-A	3.4807	eV	356.20	nm	f=0.0393	<S**2>=0.000
Excited	State	13:	Singlet-A	3.5140	eV	352.83	nm	f=0.0070	<S**2>=0.000
Excited	State	14:	Singlet-A	3.5472	eV	349.53	nm	f=0.0031	<S**2>=0.000
Excited	State	15:	Singlet-A	3.5811	eV	346.22	nm	f=0.0322	<S**2>=0.000
Excited	State	16:	Singlet-A	3.6308	eV	341.47	nm	f=0.1100	<S**2>=0.000

Dipole moments (Debye):

P1	X = -4.2889	Y = 0.1776	Z = 0.0000	Total = 4.2926
P2	X = -1.0659	Y = -13.9104	Z = -1.3859	Total = 14.0198
P3	X = 12.9600	Y = 14.1318	Z = 2.1452	Total = 19.2943

P1

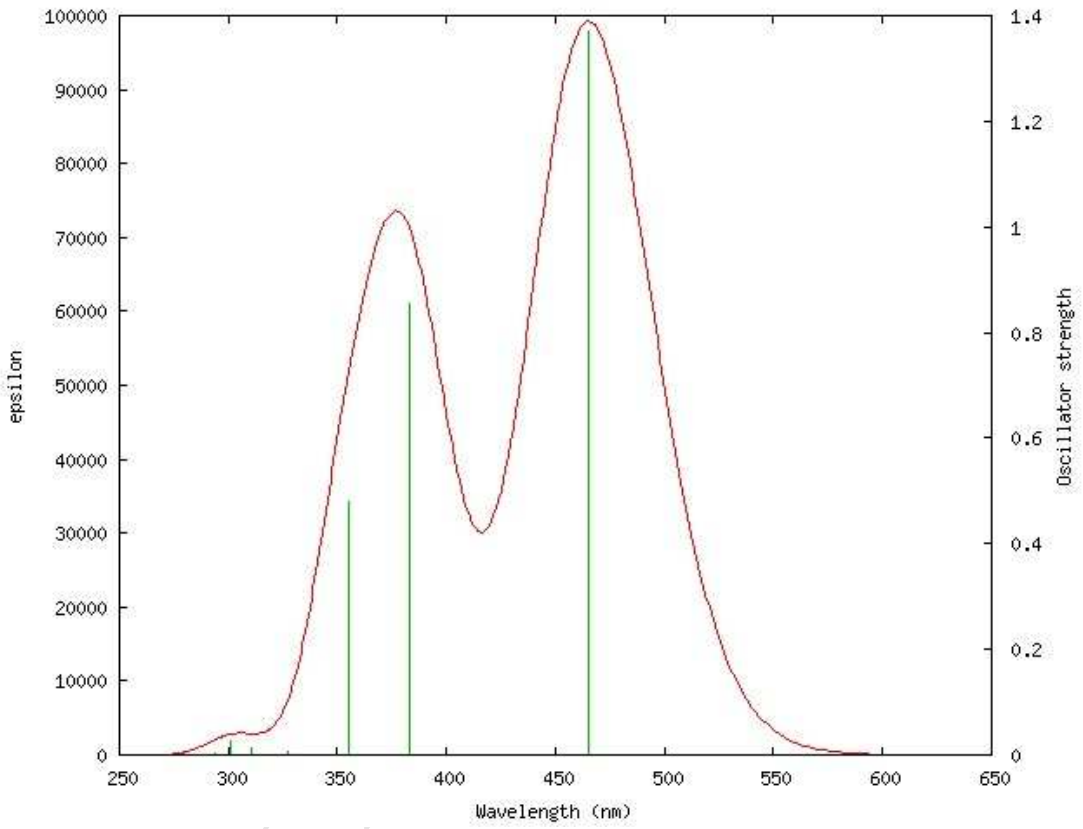

P2

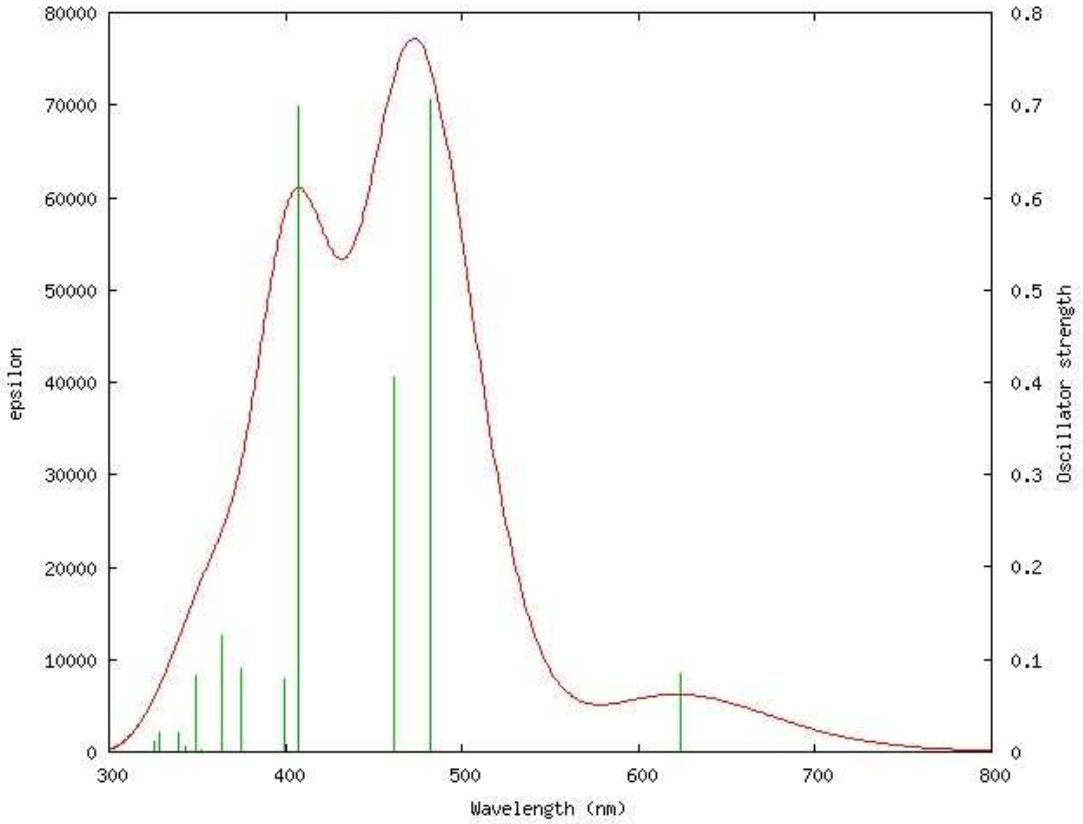
epsilon
Oscillator strength
Wavelength (nm)
0
10000
20000
30000
40000
50000
60000
70000
80000
0
0.1
0.2
0.3
0.4
0.5
0.6
0.7
0.8
300
400
500
600
700
800

P3

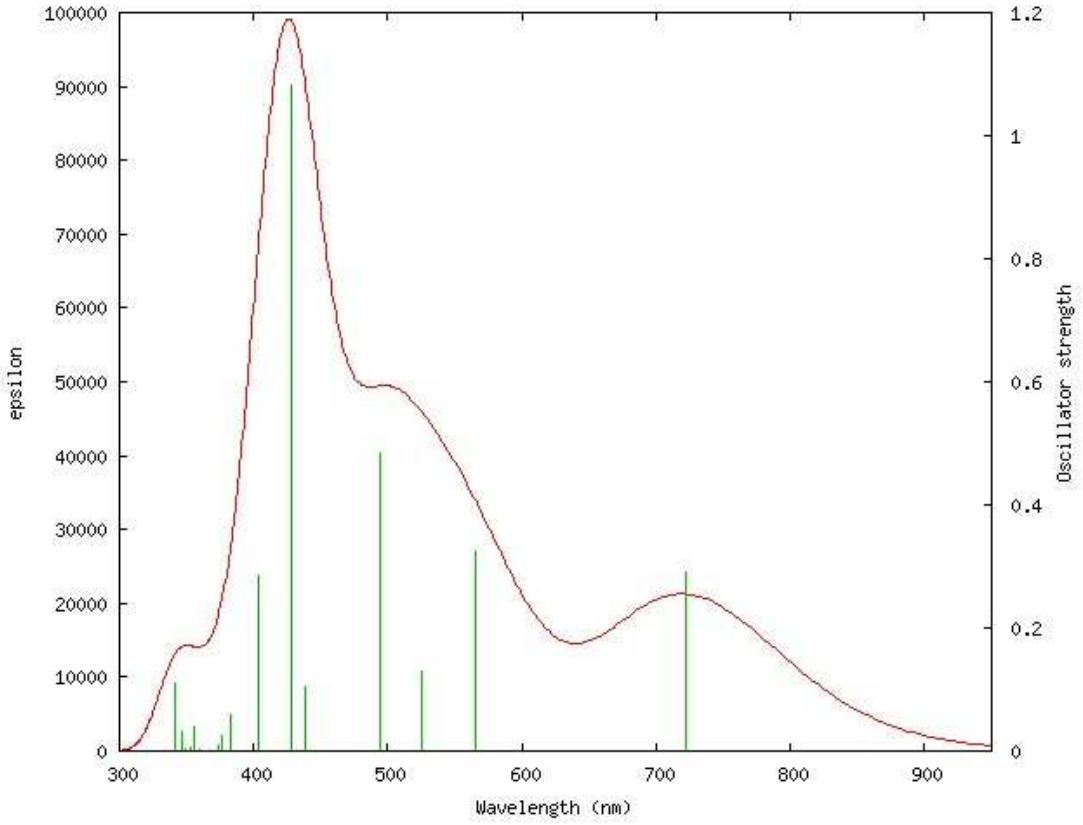
epsilon
Oscillator strength
Wavelength (nm)
0
10000
20000
30000
40000
50000
60000
70000
80000
90000
100000
0
0.2
0.4
0.6
0.8
1
1.2
300
400
500
600
700
800
900

Section S3

PESA curves

P1

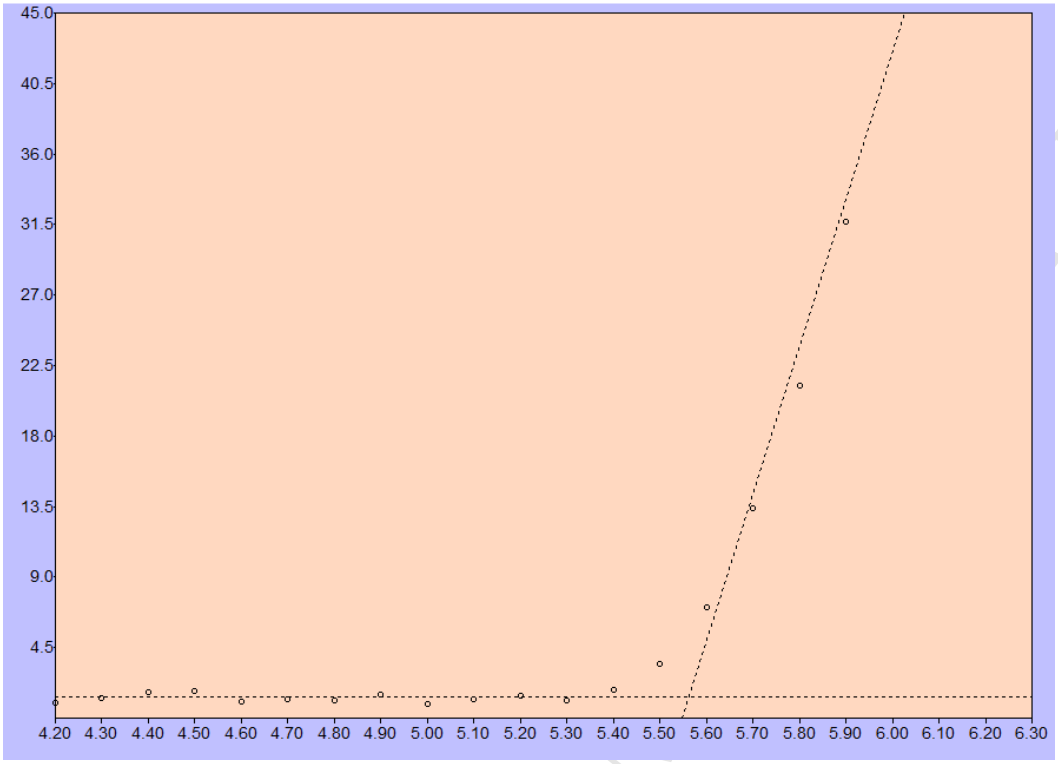

P2

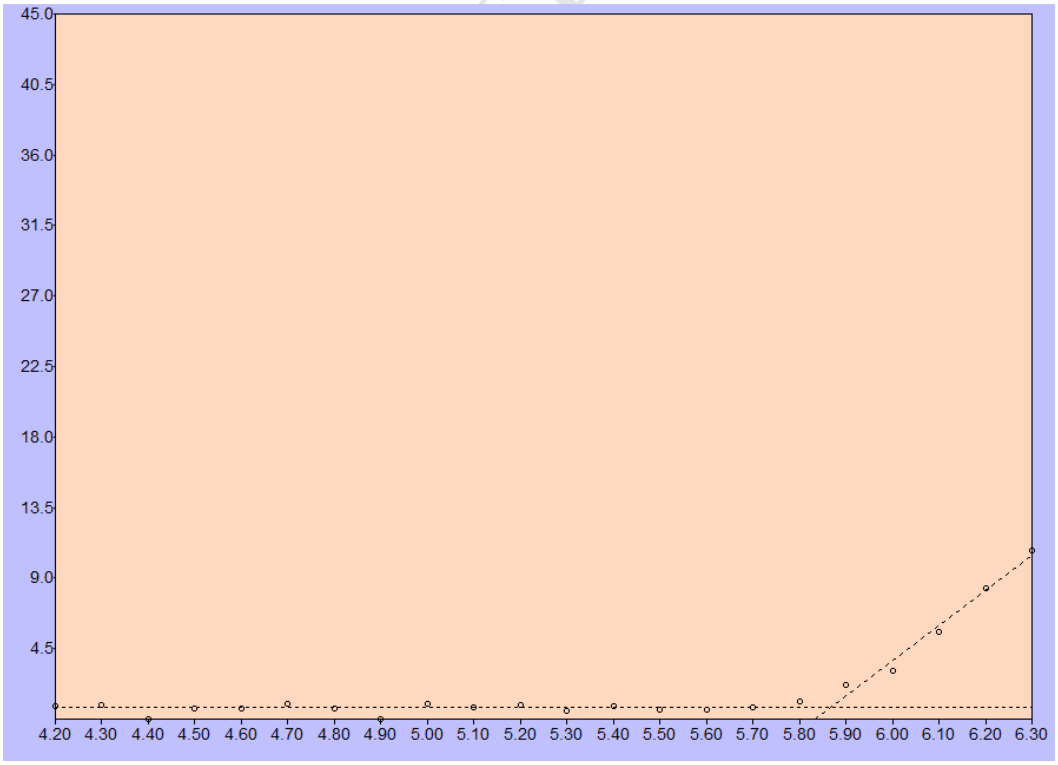

P3

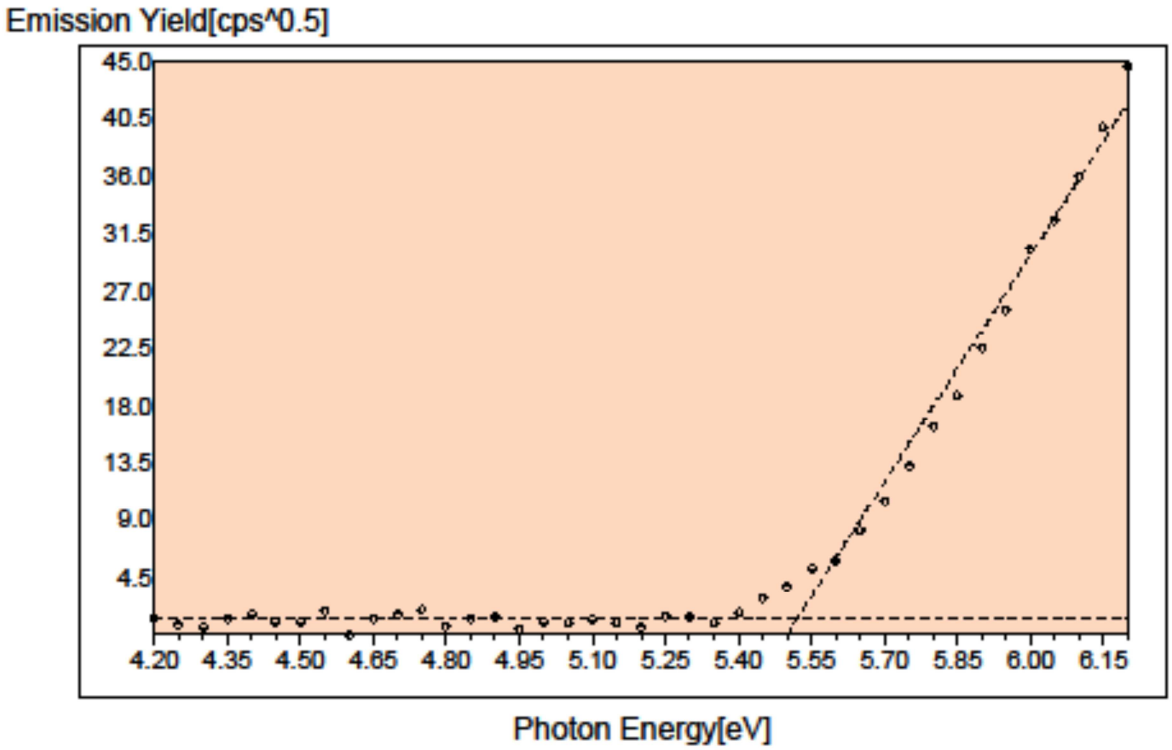
Emission Yield[cps^0.5]
45.0
40.5
36.0
31.5
27.0
22.5
18.0
13.5
9.0
4.5
4.20 4.35 4.50 4.65 4.80 4.95 5.10 5.25 5.40 5.55 5.70 5.85 6.00 6.15
Photon Energy[eV]

$PC_{61}BM$

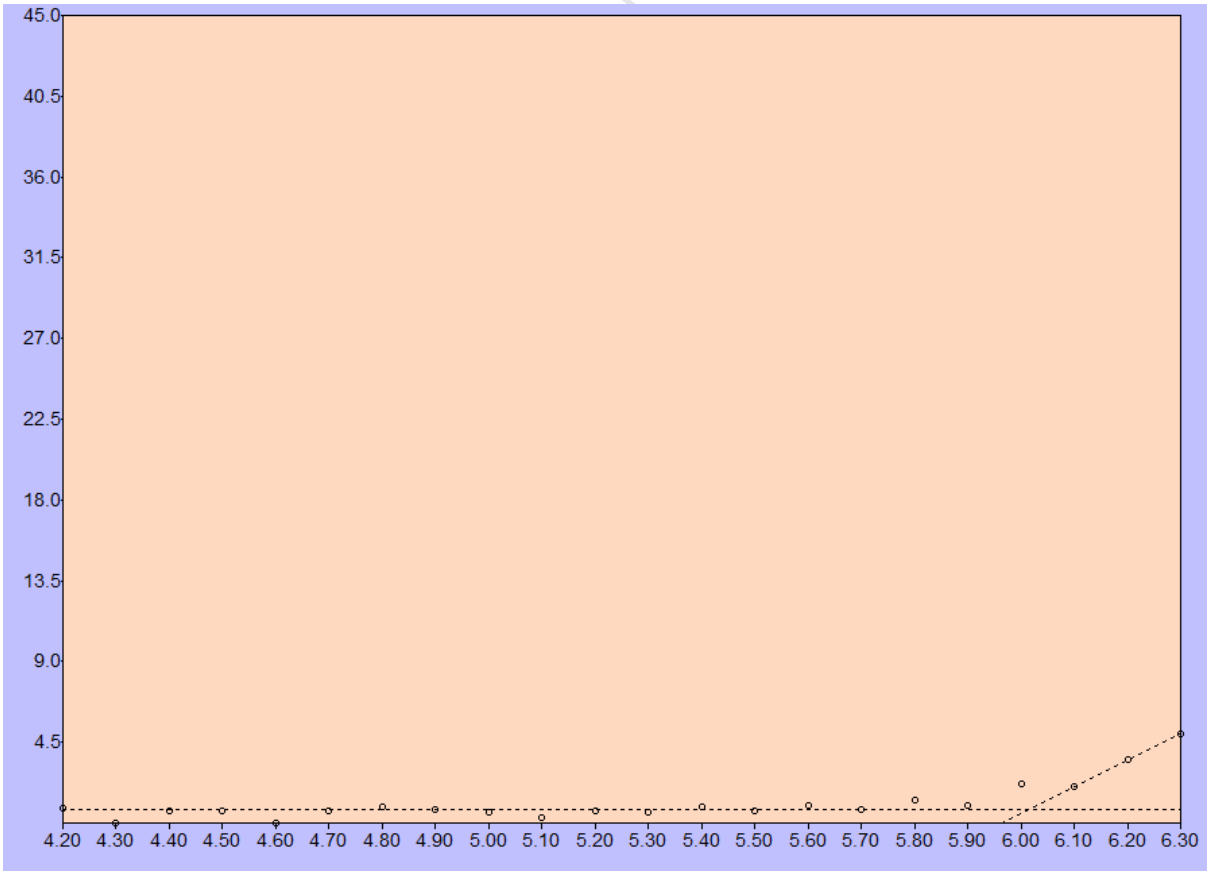
45.0
40.5
36.0
31.5
27.0
22.5
18.0
13.5
9.0
4.5
4.20 4.30 4.40 4.50 4.60 4.70 4.80 4.90 5.00 5.10 5.20 5.30 5.40 5.50 5.60 5.70 5.80 5.90 6.00 6.10 6.20 6.30

Section S4

Cyclic-voltammetry data:

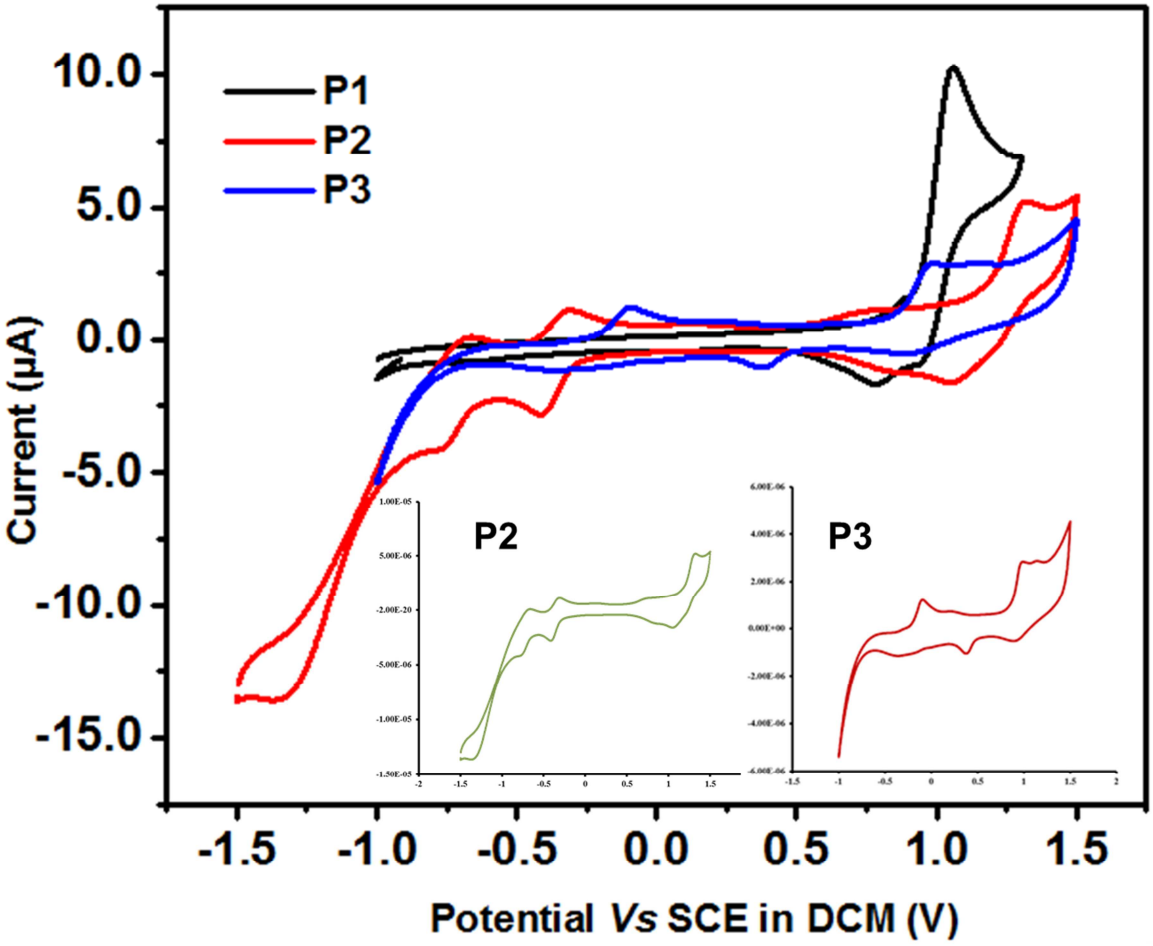

Compound	$E_{(onset)}$ (V) Ox	$E_{(onset)}$ (V) red	LUMO = (ev) -[E_{red}+4.8]	HOMO = (ev) -[E_{ox}+4.8]	E_g= (HOMO-LUMO)
P1	0.71	-0.85	-3.95	-5.51	1.56
P2	1.01	-0.13	-4.67	-5.81	1.14
p3	0.84	-0.32	-4.48	-5.64	1.16

Section S5

Overlaid TGA spectra of **P1**, **P2** and **P3** showing their thermal stability

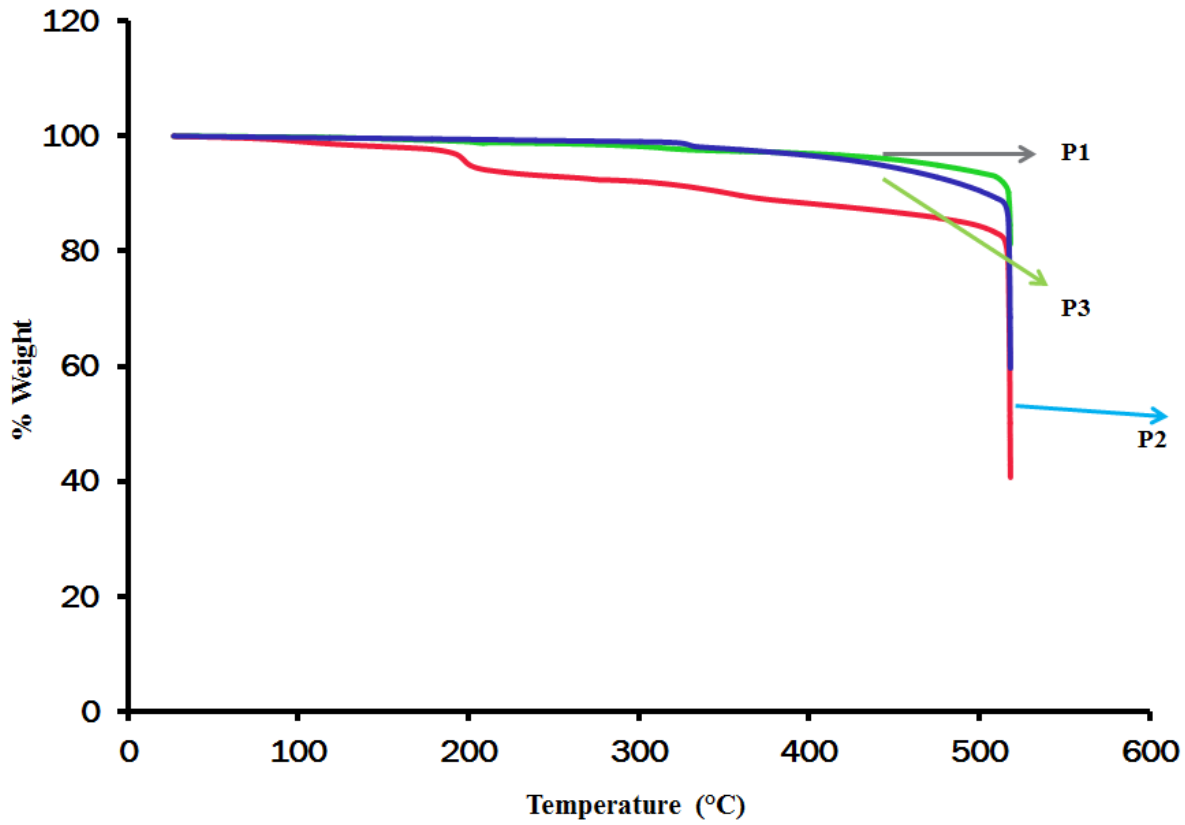

Table S1 Photovoltaic cell parameters for P3HT: **P1/P2/P3** blends

Dye	**Testing conditions**	**Blend film thickness**	V_{oc} **(V)**	J_{sc} **(mA/cm^2)**	***FF***	**Best PCE (%)**	**Average PCE (± std dev)[d] (%)**
P1	1: 1 P3HT[a]	62	1.03	5.70	0.39	2.28	2.19 (± 0.06)
P2	1: 1 P3HT[a]	63	0.93	6.78	0.59	3.75	3.64 (± 0.08)
P3	1: 1 P3HT[a]	60	0.83	8.95	0.57	4.21	4.09 (± 0.11)
$PC_{61}BM$	1: 1 P3HT[b]	63	0.56	8.66	0.63	3.08	2.98 (± 0.06)
P2	2: 1 P3HT[c]	62	0.70	3.58	0.51	1.27	1.11 (± 0.12)
P3	2: 1 P3HT[c]	64	0.58	7.43	0.37	1.60	1.49 (± 0.08)

[a] As-cast blend (P3HT: **P1**/**P2**/**P3** 1: 1); [b] A standard P3HT: $PC_{61}BM$ device afforded 3.08% efficiency, thereby indicating the reliability of our device fabrication strategy; [c] BHJ devices with specified weight ratio (donor: acceptor 1: 2). Overall device structure is ITO/PEDOT:PSS (38 nm)/active layer/Ca (20 nm)/Al (100 nm) with an active layer thickness of around 60 nm; [d] A total of ten devices were made for each combination; cell area = 0.2 cm^2

Section S6

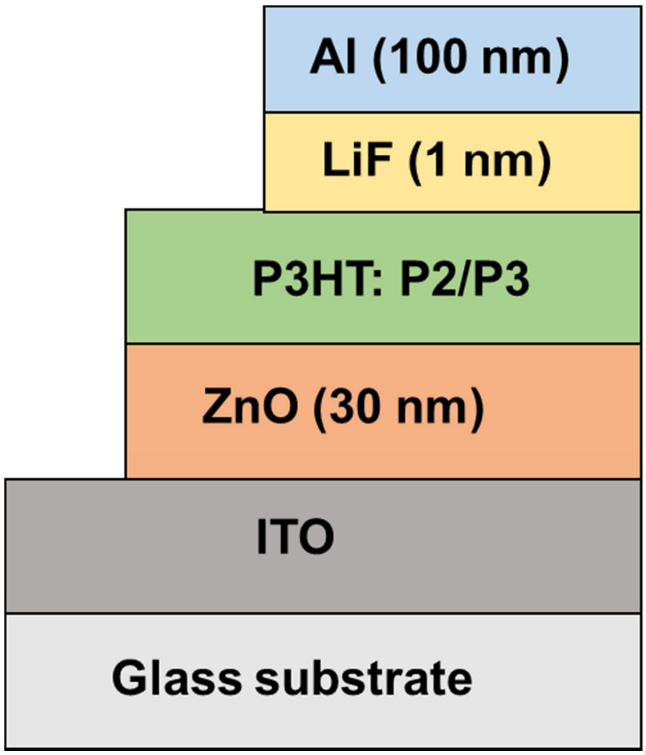
Al (100 nm)
LiF (1 nm)
P3HT: P2/P3
ZnO (30 nm)
ITO
Glass substrate

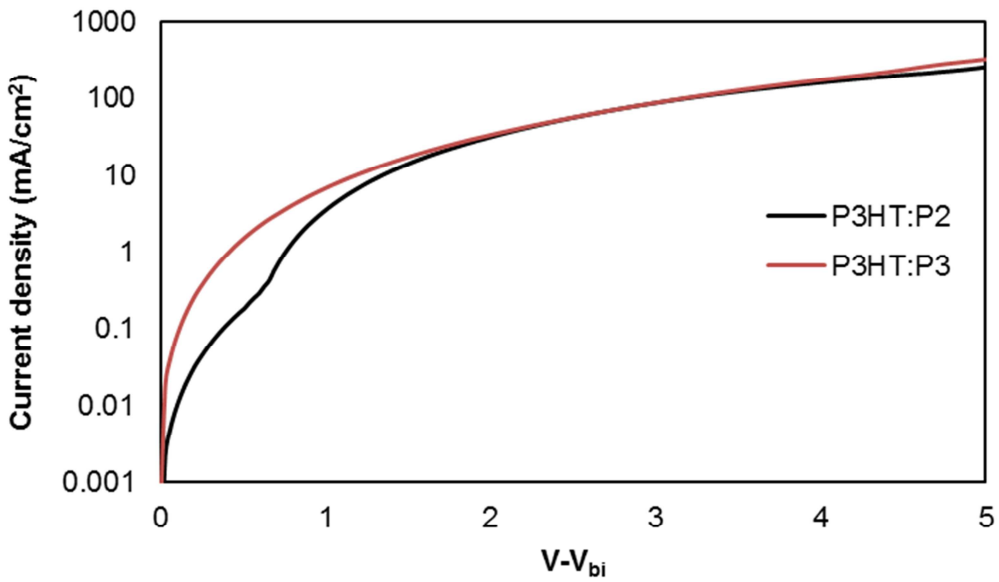
Current density (mA/cm²)
1000
100
10
1
0.1
0.01
0.001
0
1
2
3
4
5
V-V_bi
P3HT:P2
P3HT:P3

SCLC details: Device sketch of the electron-only devices (upper) that was used to study SCLC method and the current–voltage characteristics (lower) that were applied to the Mott-Gurney equation to calculate electron mobilities of the blend films of P3HT: **P2** and P3HT: **P3**.

Experimental spectra

FT-IR of compound 5:

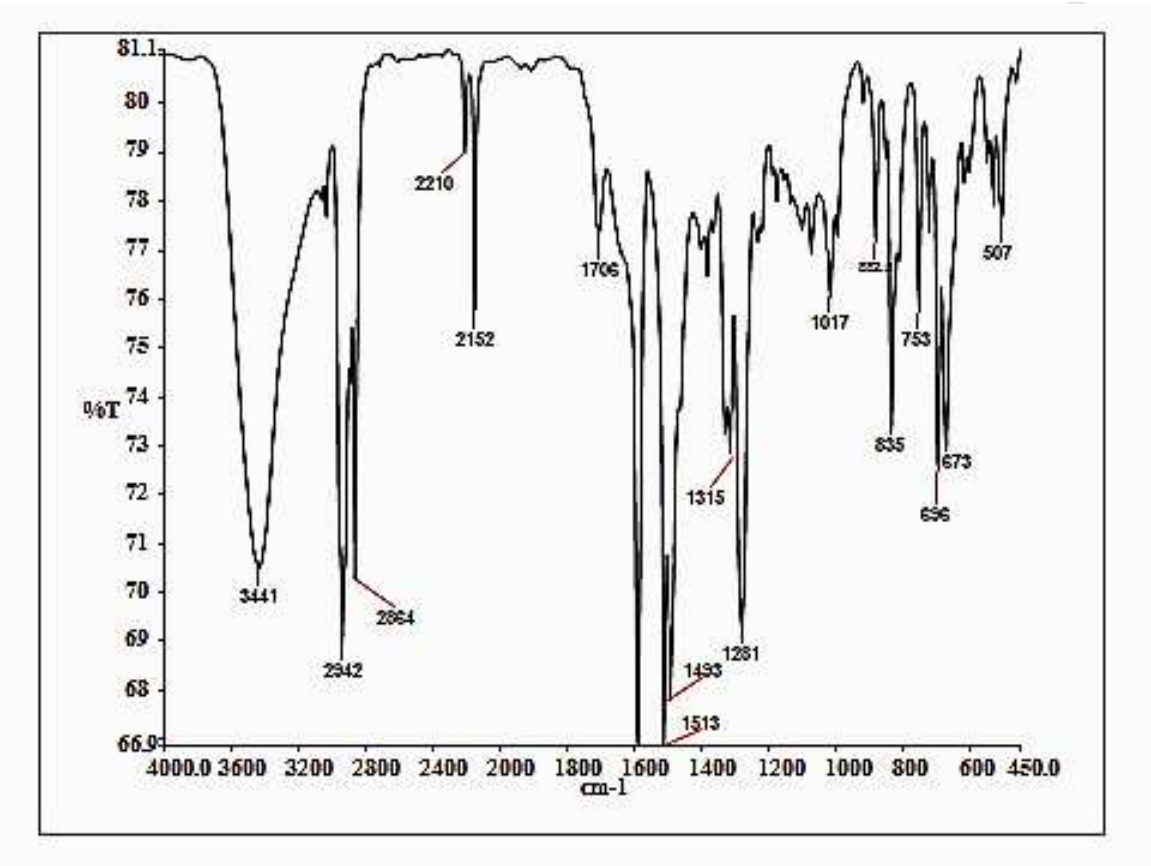

^{1}H NMR of compound 5:

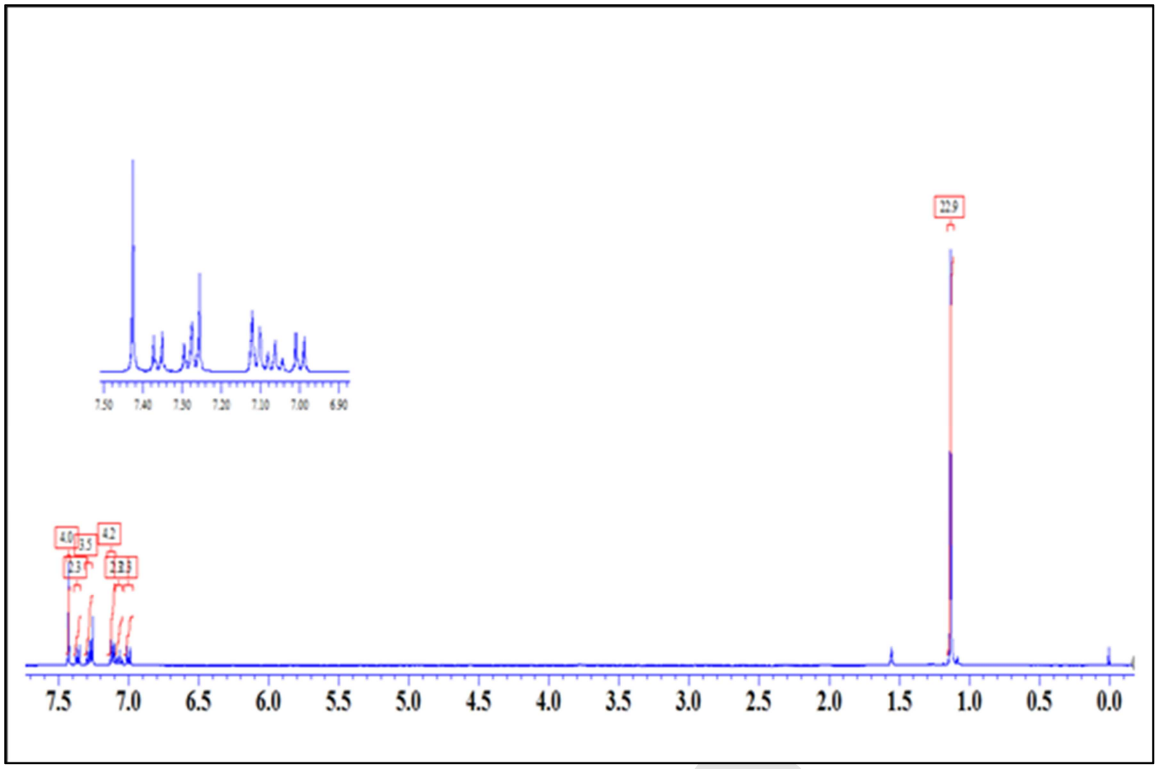

^{13}C NMR of compound 5:

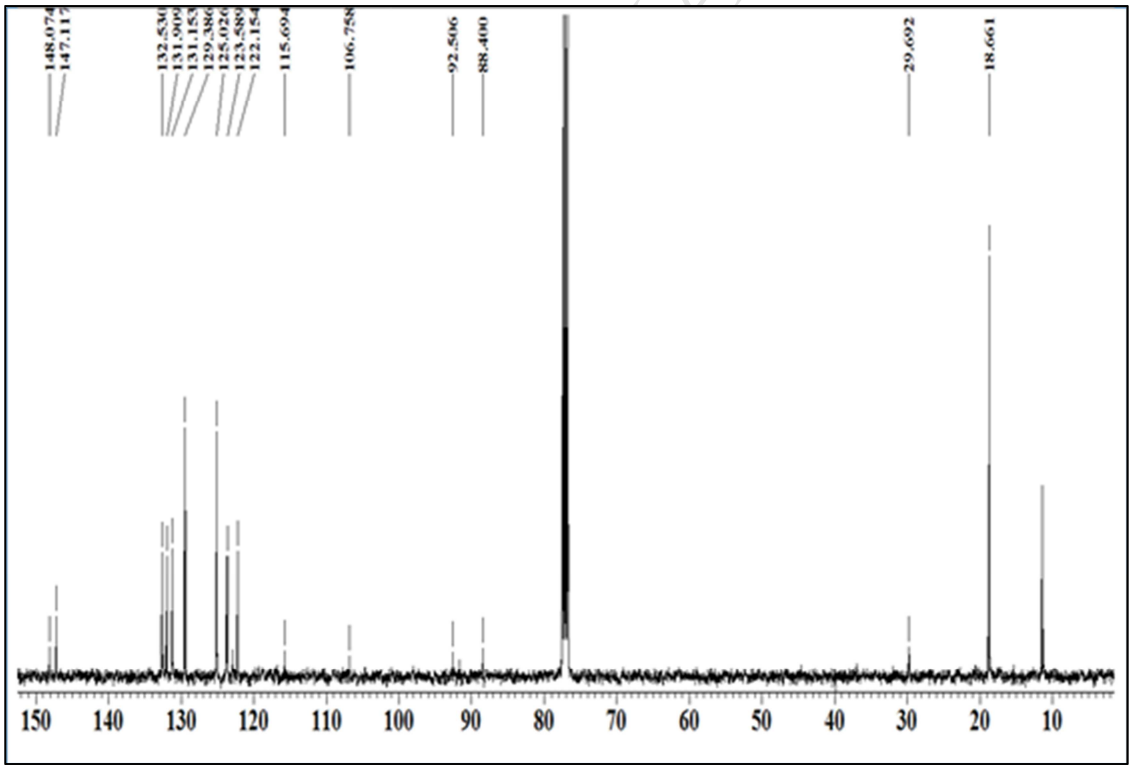

FT-IR of compound 6:

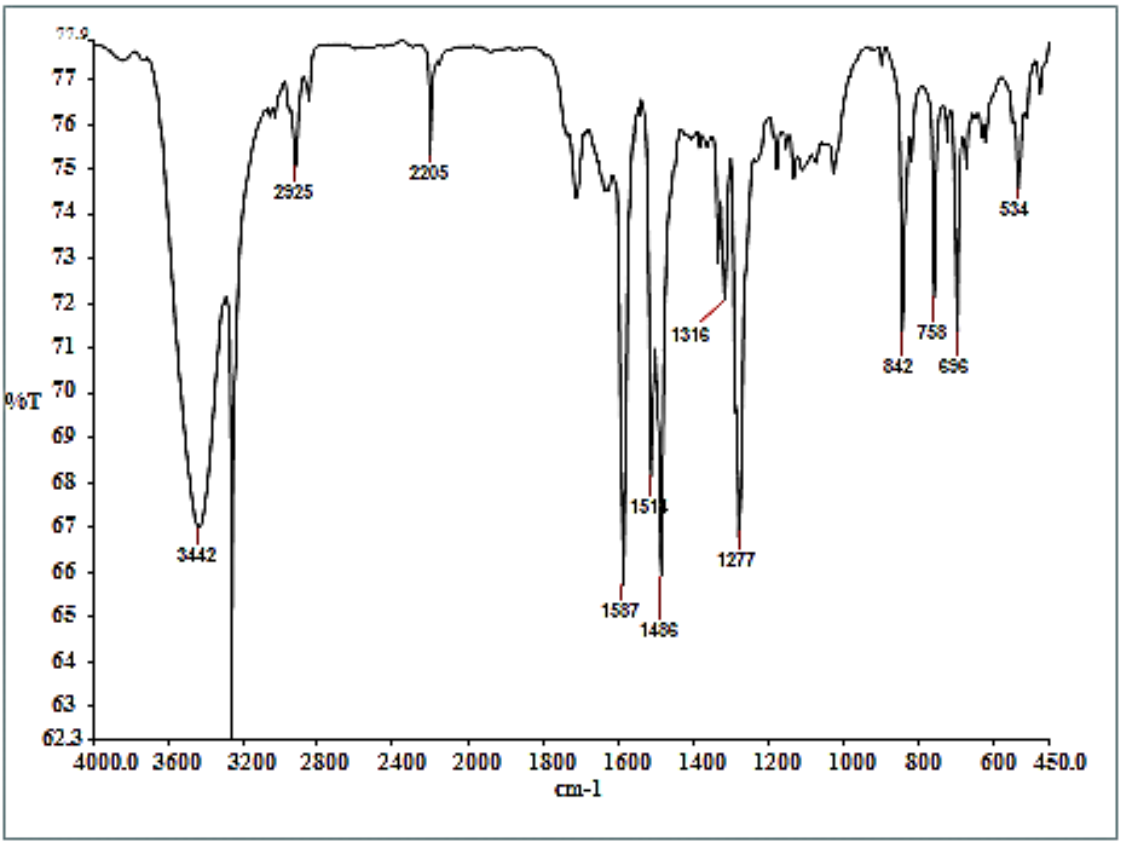

^{1}H NMR of compound 6:

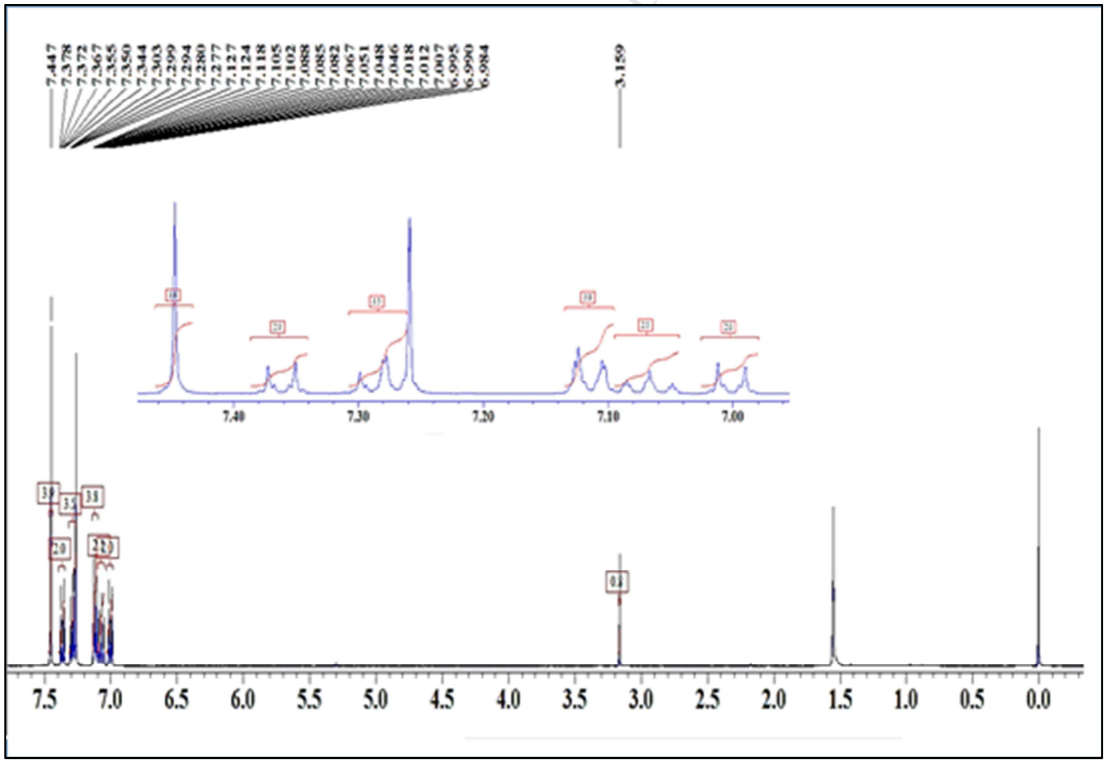

^{13}C NMR of compound 6:

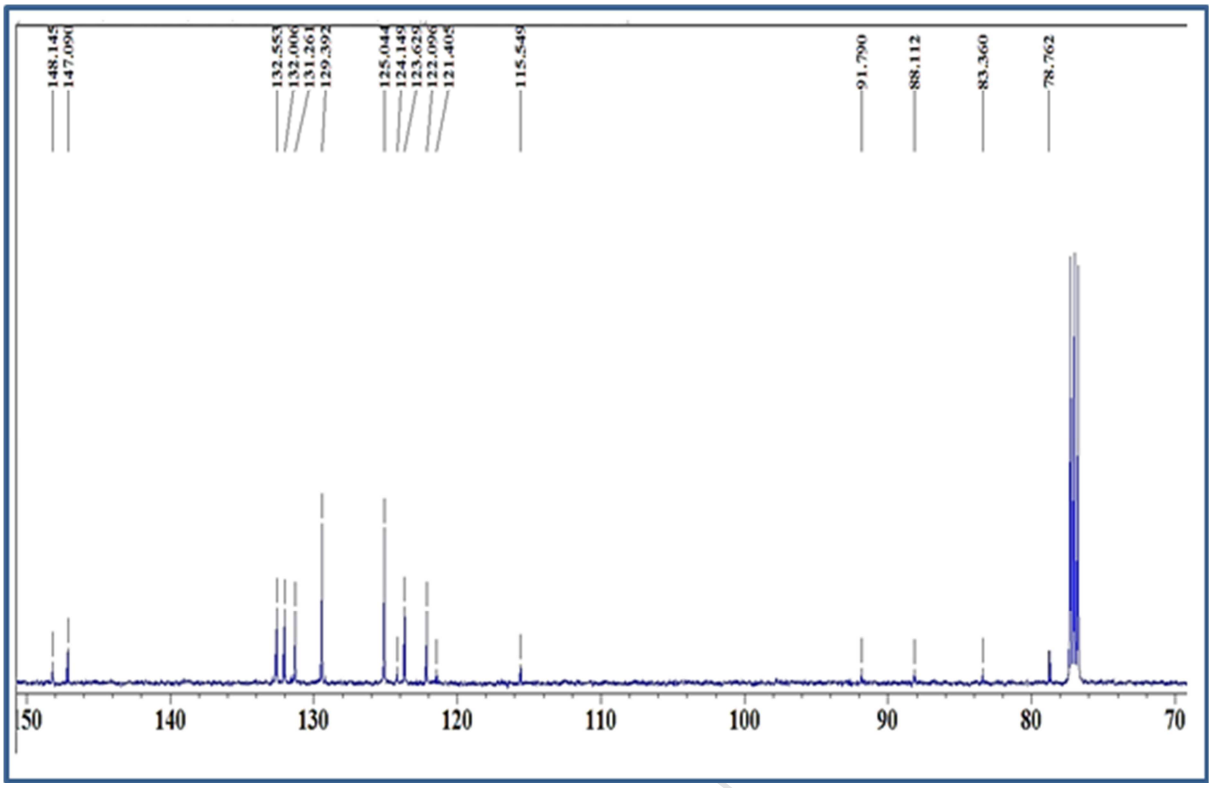

0

0

FT-IR of compound P1:

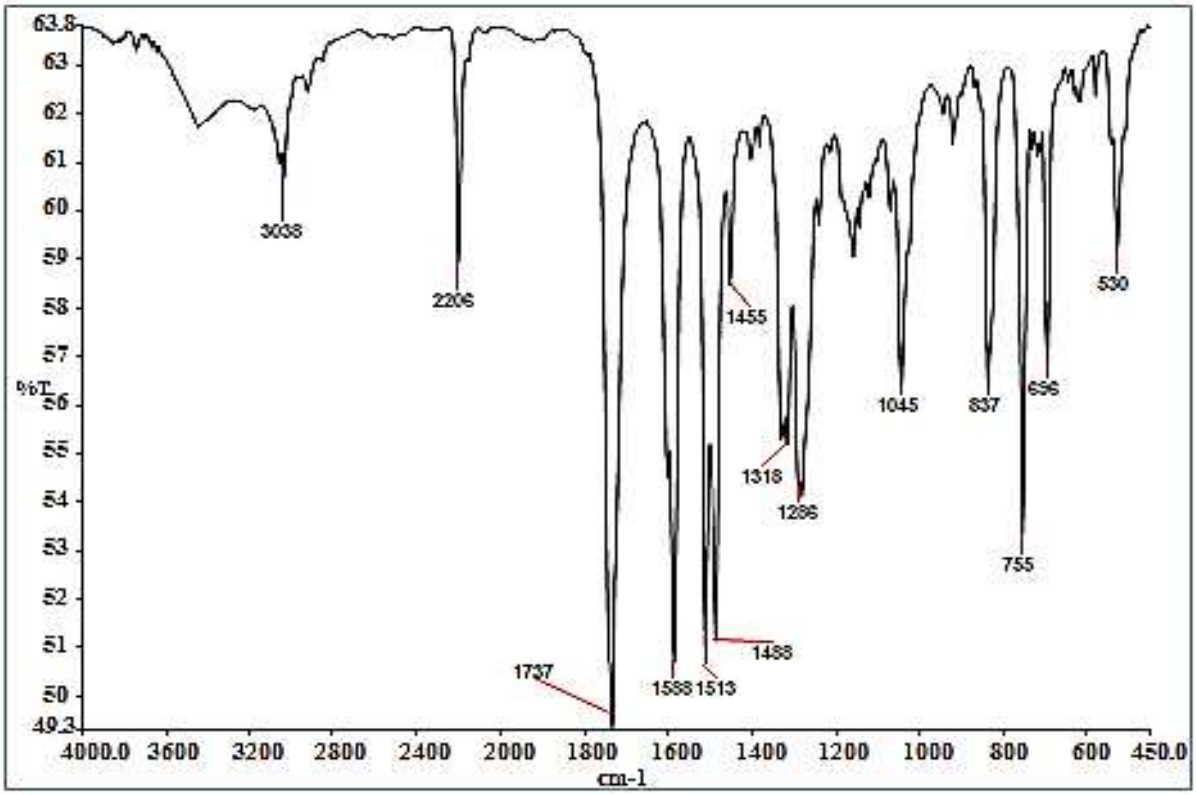

^{1}H NMR of compound P1:

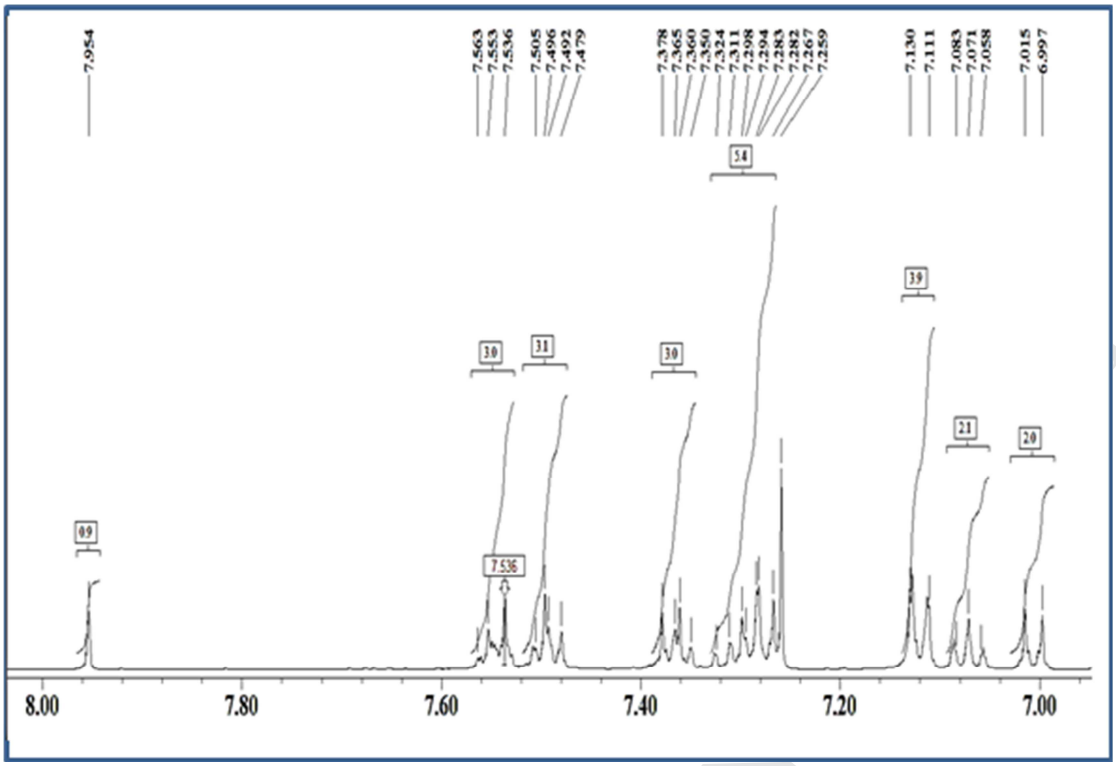

^{13}CNMR of compound P1:

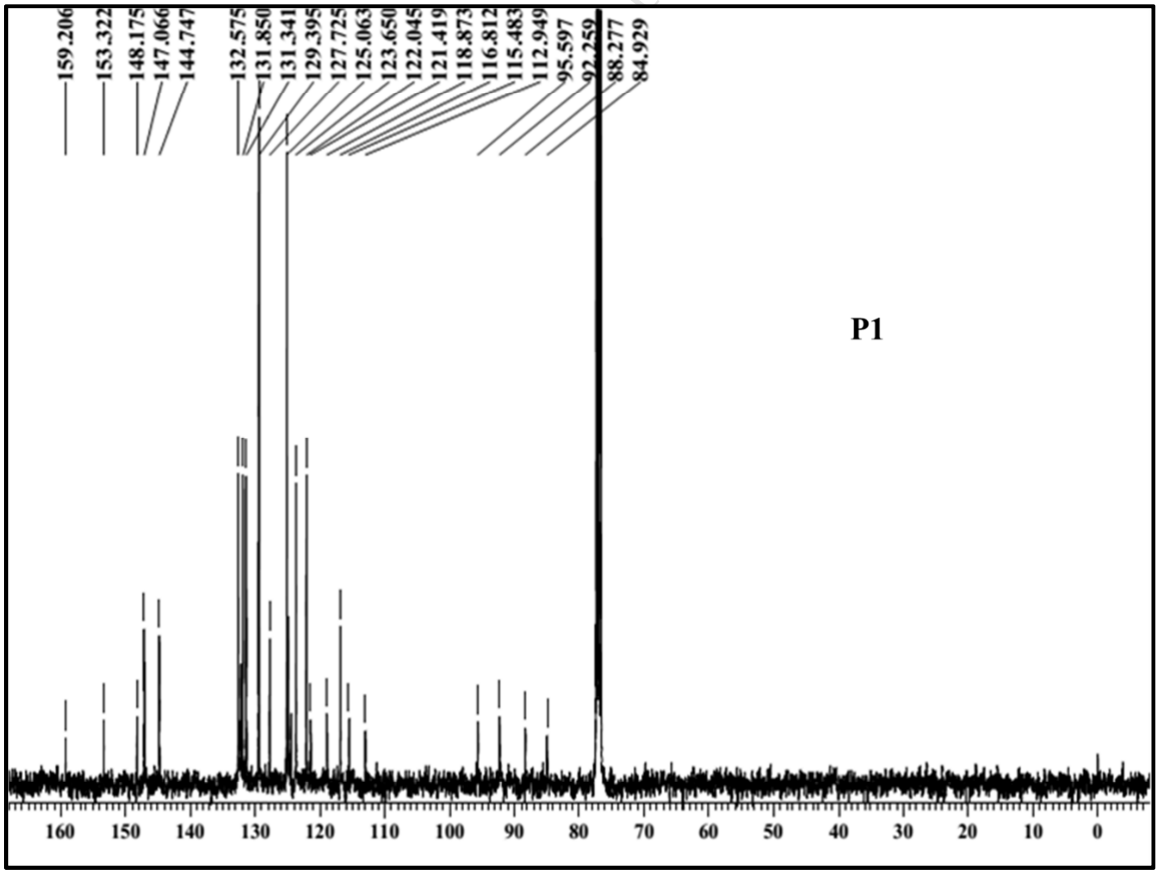

FT-IR of compound P2:

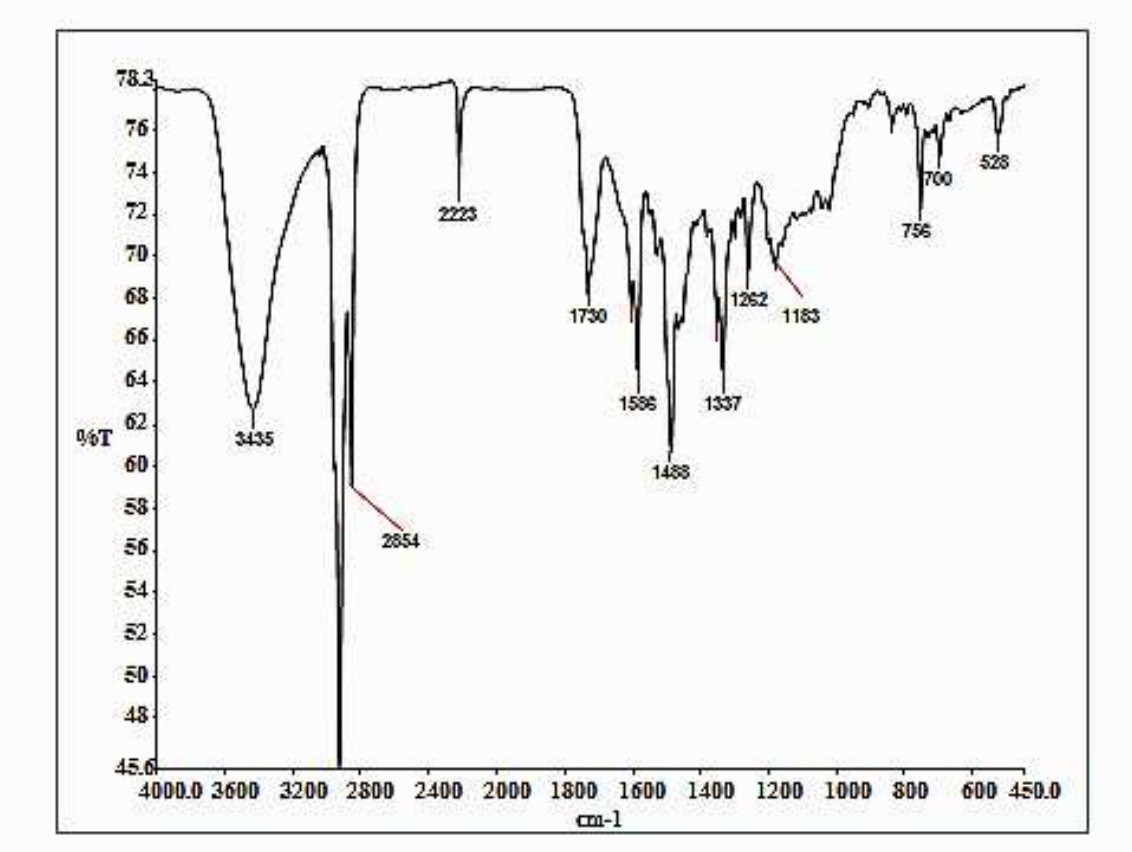

^{1}H NMR of compound P2:

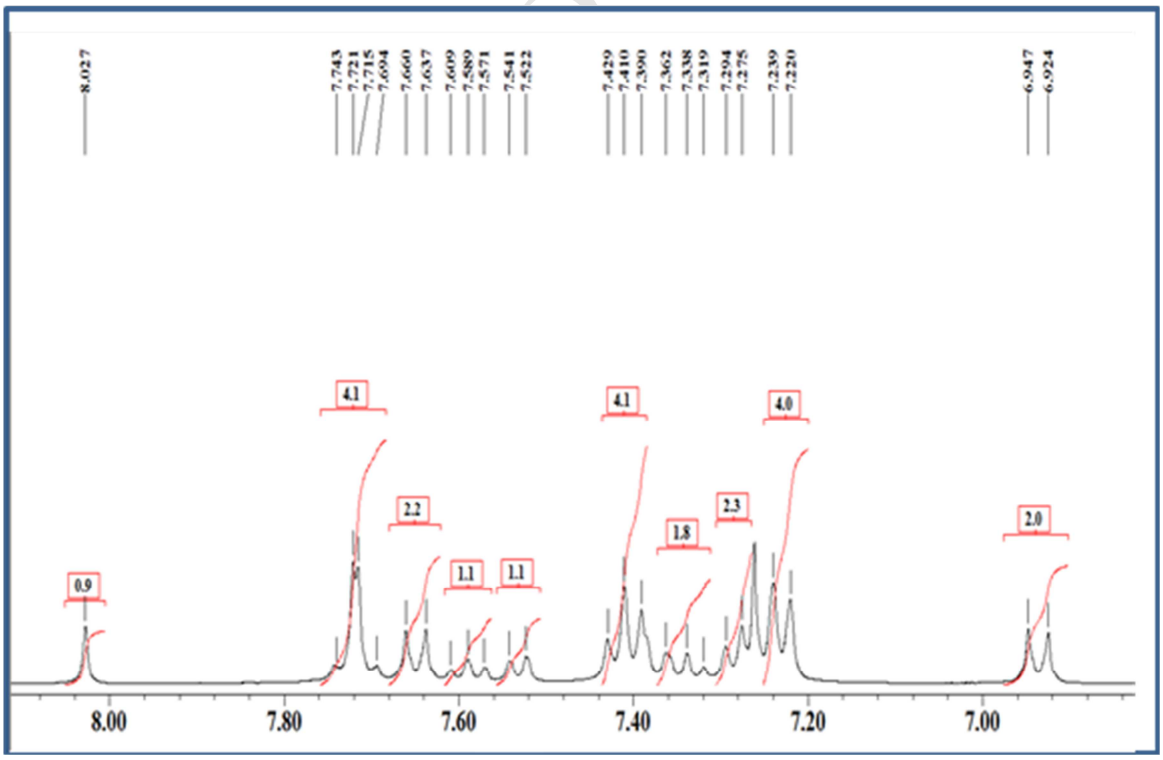

^{13}C NMR of compound P2:

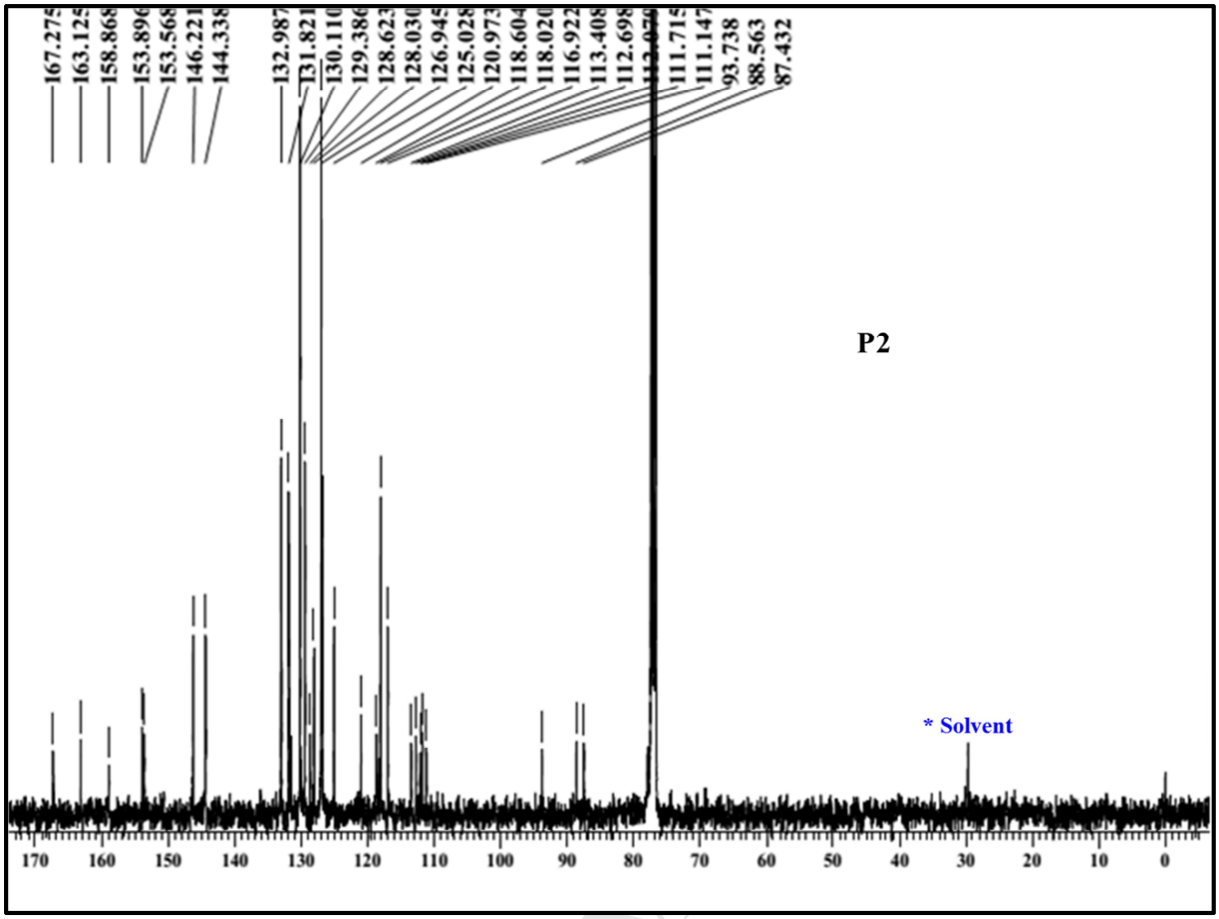

FT-IR of compound P3:

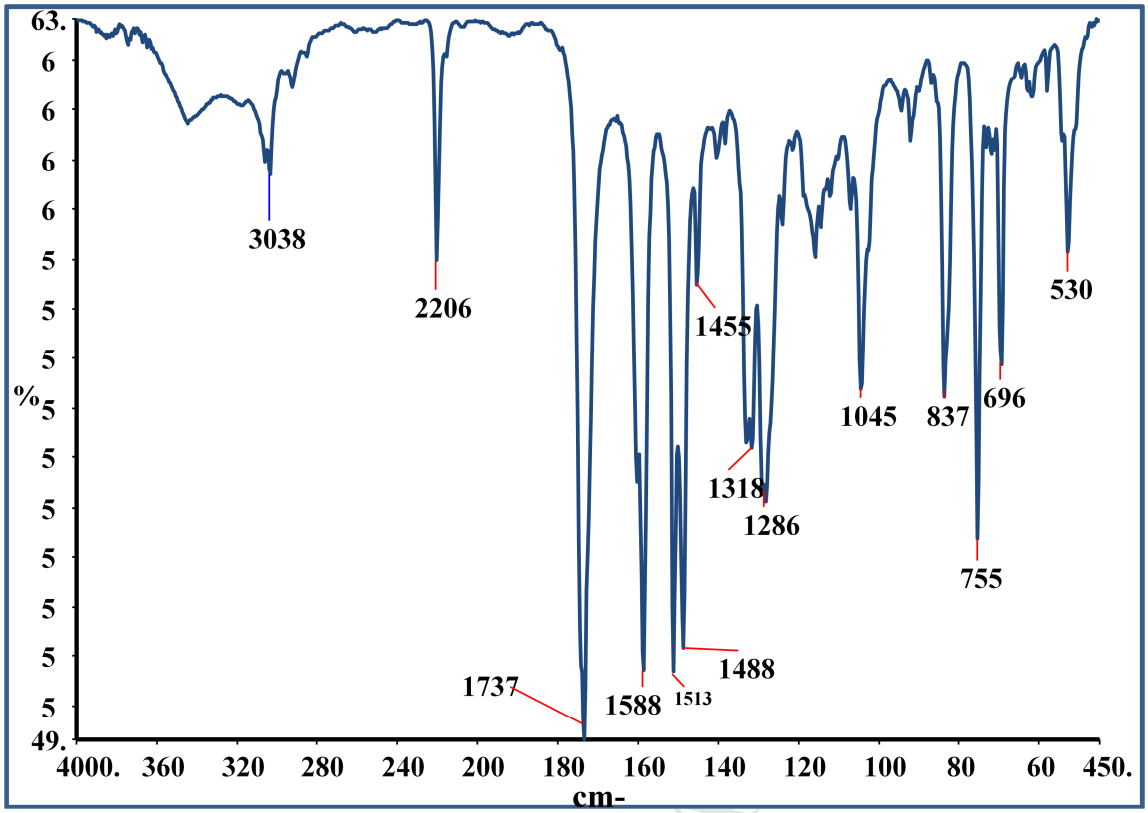

^{1}H NMR of compound P3:

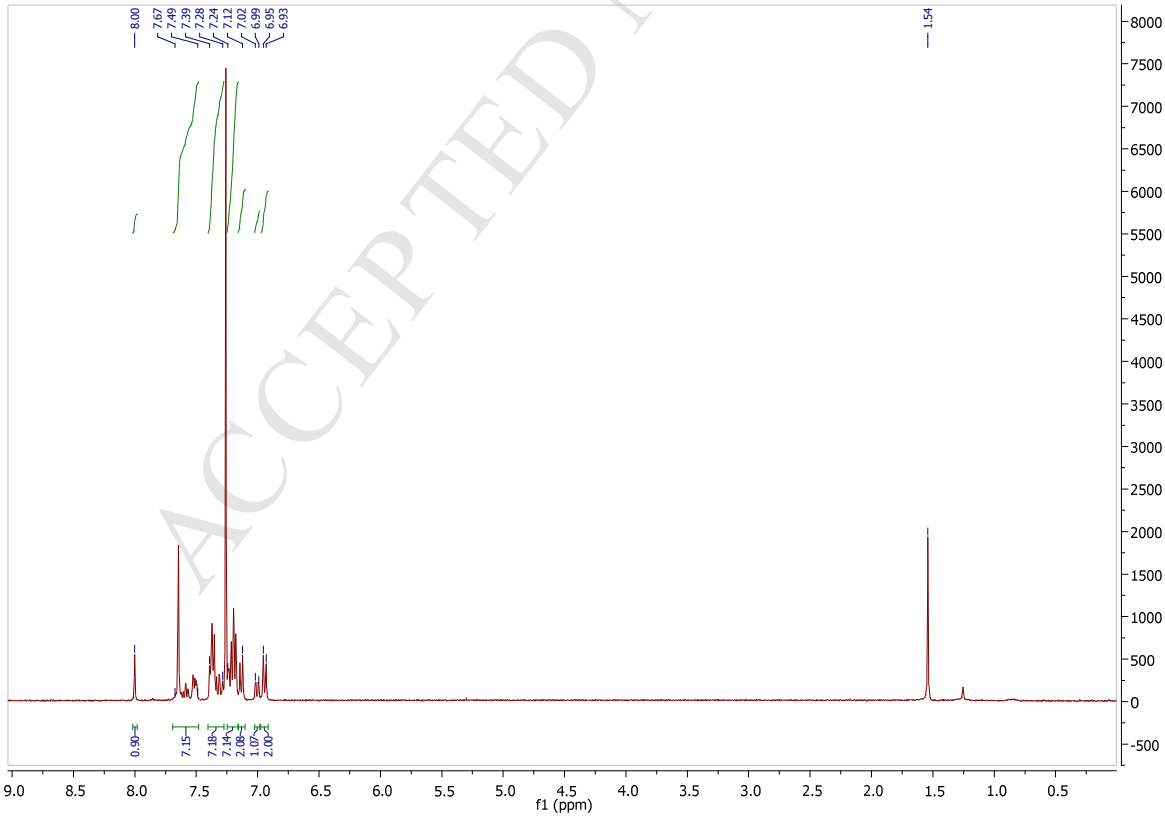

^{13}C NMR of compound P3:

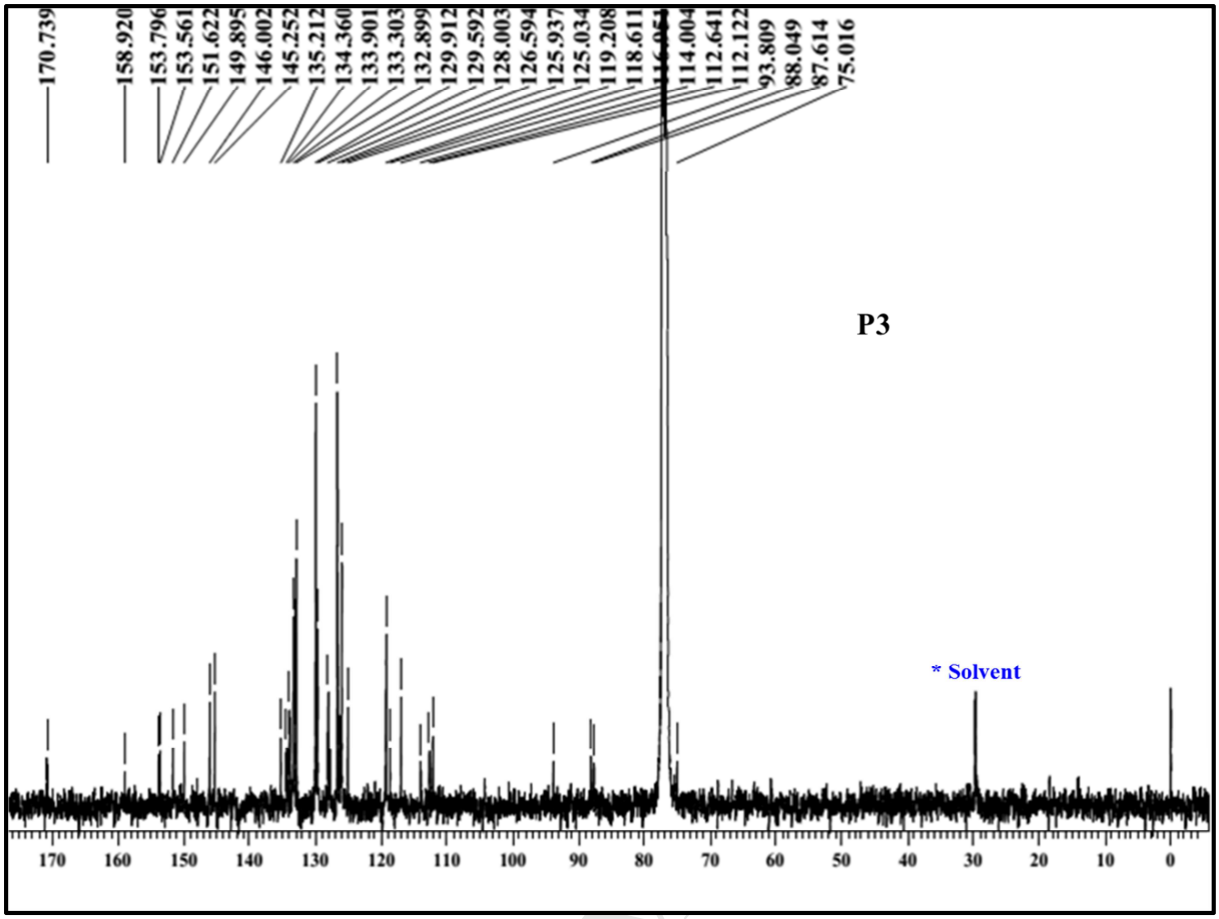

Research Highlights

- The first effort to utilize chromen-2-one for generating non-fullerene acceptors
- Generation of D-A1-A module using chromen-2-one, and tetracyanoethylene/tetracyanoquinodimethane units
- Comparison of D-A1-A and D-A designs for optoelectronic and photovoltaic properties
- Use of chromen-2-one/tetracyanoquinodimethane combination for improved light-harvesting
- One of the materials (**P3**) demonstrated highest efficiency of 4.21%